Mitochondrial impairments contribute to Spinocerebellar ataxia type 1 progression and can be ameliorated by the mitochondria-targeted antioxidant MitoQ

David M. Stucki, Céline Ruegsegger, Silvio Steiner, Julika Radecke, Michael P. Murphy, Benoît Zuber, Smita Saxena

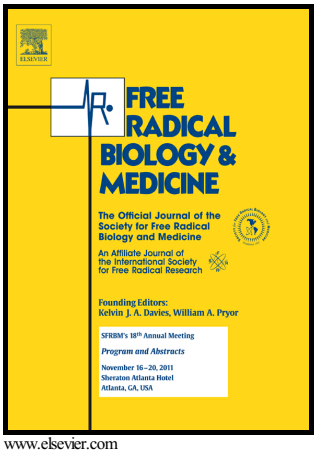

www.elsevier.com

PII: S0891-5849(16)30325-2
DOI: http://dx.doi.org/10.1016/j.freeradbiomed.2016.07.005
Reference: FRB12928

To appear in: *Free Radical Biology and Medicine*

Received date: 15 April 2016
Revised date: 23 June 2016
Accepted date: 5 July 2016

Cite this article as: David M. Stucki, Céline Ruegsegger, Silvio Steiner, Julika Radecke, Michael P. Murphy, Benoît Zuber and Smita Saxena, Mitochondrial impairments contribute to Spinocerebellar ataxia type 1 progression and can be ameliorated by the mitochondria-targeted antioxidant MitoQ, *Free Radical Biology and Medicine,* http://dx.doi.org/10.1016/j.freeradbiomed.2016.07.005

Mitochondrial impairments contribute to Spinocerebellar ataxia type 1 progression and can be ameliorated by the mitochondria-targeted antioxidant MitoQ

David M. Stucki[1,4], Céline Ruegsegger[1,4], Silvio Steiner[1], Julika Radecke[2,4], Michael P. Murphy[3], Benoît Zuber[2], Smita Saxena[1,*]

[1]Institute of Cell Biology, University of Bern, Bern, Switzerland

[2]Institute of Anatomy, University of Bern, Bern, Switzerland

[3] Medical Research Council, Mitochondrial Biology Unit, Cambridge, United Kingdom

[4]Graduate School for Cellular and Biomedical Sciences, University of Bern, Bern, Switzerland

[*]Corresponding author: Smita Saxena, Institute of Cell Biology, Baltzerstrasse 4, CH-3012 Bern, Switzerland. Tel: +41-31-631-4620, fax: +41-31-631-4431, smita.saxena@izb.unibe.ch

Short title: MitoQ improves SCA1 pathology

Abstract

Spinocerebellar ataxia type 1 (SCA1), due to an unstable polyglutamine expansion within the ubiquitously expressed Ataxin-1 protein, leads to the premature degeneration of Purkinje cells (PCs), decreasing motor coordination and causing death within 10-15 years of diagnosis. Currently, there are no therapies available to slow down disease progression. As secondary cellular impairments contributing to SCA1 progression are poorly understood, here, we focused on identifying those processes by performing a PC specific proteome profiling of $Sca1^{154Q/2Q}$ mice at a symptomatic stage. Mass spectrometry analysis revealed prominent alterations in mitochondrial proteins. Immunohistochemical and serial block-face scanning electron microscopy analyses confirmed that PCs underwent age-dependent alterations in mitochondrial morphology. Moreover, colorimetric assays demonstrated impairment of the electron transport

chain complexes (ETC) and decrease in ATPase activity. Subsequently, we examined whether the mitochondria-targeted antioxidant MitoQ could restore mitochondrial dysfunction and prevent SCA1-associated pathology in $Sca1^{154Q/2Q}$ mice. MitoQ treatment both presymptomatically and when symptoms were evident ameliorated mitochondrial morphology and restored the activities of the ETC complexes. Notably, MitoQ slowed down the appearance of SCA1-linked neuropathology such as lack of motor coordination as well as preventing oxidative stress-induced DNA / RNA damage and PC loss. Our work identifies a central role for mitochondria in PC degeneration in SCA1 and provides evidence for the supportive use of mitochondria-targeted therapeutics in slowing down disease progression.

Keywords, Spinocerebellar ataxia type 1, Purkinje cells, mitochondria, oxidative stress, Electron transport chain (ETC) activities, neurodegeneration, antioxidant MitoQ.

Introduction

Spinocerebellar ataxia type 1 (SCA1) belongs to one of the major groups of autosomal dominant hereditary cerebellar ataxia. It is a fatal cerebellum-associated neurodegenerative disease (ND) where patients manifest their first symptoms in their mid-30s to 40s and die within 10-15 years of diagnosis (Burk et al., 1996). The disease is associated with an unstable trinucleotide CAG repeat expansion in the open reading frame of the ataxin-1 gene. This specific CAG repeat expansion leads to the expression of an expanded polyglutamine (polyQ) tract in the mutant Ataxin-1 protein (ATXN1), thereby acquiring a toxic gain-of-function property (Orr, 2012; Zoghbi, 1995; Zoghbi and Orr, 1995, 2009). Similar to other polyQ related SCAs, pathological hallmarks of SCA1 involves premature degeneration of Purkinje cell (PC) dendrites, dendritic spines and PC soma that lead to motor incoordination, gait disorder, ataxia, dysarthria, dysphagia and massive cerebellar atrophy (Burk et al., 1996; Koeppen, 1991; Zoghbi and Orr, 2009). Several mutant SCA1 transgenic mouse models, which reliably replicate human pathology, have been generated and those mice have facilitated the understanding of disease mechanisms that may be involved in the development of the pathology. Knock-in mice harboring 154 CAG repeats in the ataxin-1 locus ($Sca1^{154Q/2Q}$) (Watase et al., 2002) and transgenic mice that overexpress a mutant ATXN1 form with 82 CAG repeats selectively within PCs (B05[82Q]) (Burright et al., 1995) have been used in the past to understand the physiological role of ATXN1 as well as SCA1-associated pathomechanisms. Interestingly, it was also revealed that the overexpression of the normal form of ATXN1, produces similar toxic effects (Fernandez-Funez et al., 2000),

suggesting that an activity or interaction of ATXN1 in excess is sufficient to cause neuronal dysfunction.

NDs are an ever increasing socio-economic burden to the developed world. Despite substantial efforts in recent decades to understand mechanisms that determine the disease process in ND, no therapy is available to halt their progression and the only treatment option is to subdue symptoms. Currently, there is an urgent need for the development of valid therapies to slow down or stop neuronal degeneration thereby providing a better quality of life to patients. This lack of therapies is due at least in part to a substantial lacuna in our understanding of the early disease mechanisms.

A well accepted and conserved feature of all neurons that degenerate is that they have an exceptional demand for energy in order to maintain their membrane potential and generate an action potential (Calabrese et al., 2001; Schapira, 1998). Because of their limited glycolytic capacity, neurons are highly dependent on aerobic oxidative phosphorylation (OXPHOS) which is fulfilled by mitochondria located at strategic sites inside the cell and synapse. On the other hand, the OXPHOS machinery is a major producer of reactive oxygen species (ROS) which cause oxidative damage to DNA, RNA, lipids and proteins (Beal, 1996; Manfredi and Beal, 2000; Schapira, 1996). Hence, a fine-tuned regulation of OXPHOS activity and protective mechanisms against ROS including antioxidants is essential to maintain a healthy balance between energy- and ROS production. Therefore, it is not surprising that mitochondrial dysfunction and oxidative stress have been implicated in various NDs (Burte et al., 2015; Chaturvedi and Flint Beal, 2013; Karbowski and Neutzner, 2012), such as Alzheimer's disease (AD) (Friedland-Leuner et al., 2014; Simoncini et al., 2015), Parkinson's disease (PD) (Haelterman et al., 2014; Hang et al., 2015; Overk and Masliah, 2014; Ryan et al., 2015), Huntington's disease (HD) (Ayala-Pena, 2013; Guedes-Dias et al., 2015; Labbadia and Morimoto, 2013; Tsunemi and La Spada, 2012) and Amyotrophic lateral sclerosis (ALS) (Cozzolino et al., 2013; Duffy et al., 2011; Magrane and Manfredi, 2009). Importantly, in inherited recessive ataxias such as Autosomal recessive spastic ataxia of Charlevoix-Saguenay (ARSACS) or Friedreich's ataxia, mutations within mitochondria-associated proteins are the most frequent cause underlying the development of these disease (Calabrese et al., 2005; Criscuolo et al., 2015; Girard et al., 2012). These observations are not unexpected considering that PCs are amongst the most active neurons in the central nervous system and have a high energy demand that makes them particularly susceptible to mitochondrial impairment or dysfunction (Zeviani et al., 2012). Importantly, a recent study revealed that mutant ATXN1 mediates the reduction or inhibition of the high-mobility group box 1 protein (HMGB1) in mitochondria, which led to increased mitochondrial DNA damage in a SCA1

mouse model. Mitochondrial DNA damage, as well as neuropathology and a motor deficit could be rescued by viral-mediated over-expression of HMGB1 (Ito et al., 2015). However, it remained unclear when during disease progression mitochondria became functionally altered, what precise mitochondrial processes were impaired and whether those impairments contributed to SCA1 pathology.

Here, we focused on identifying processes which are specifically impaired during the appearance of SCA1-associated symptoms and contribute to disease progression. PC specific proteome profiling of Sca1$^{154Q/2Q}$ mice revealed prominent alterations in mitochondrial proteins which coincided with the symptomatic phase of the disease. Targeting mitochondrial impairments by treating Sca1$^{154Q/2Q}$ mice with a mitochondria- targeted antioxidant; MitoQ significantly restored mitochondrial functioning and ameliorated disease symptoms.

Experimental procedures

Transgenic mice

Heterozygous B6.129S-Atxn1tm1Hzo/J (Sca1$^{154Q/2Q}$) mice were obtained from Jackson Laboratory (Watase et al., 2002). Animal care, housing, ethical usage and procedure were in accordance with the Swiss Veterinary Law guidelines.

MitoQ treatment

500 μM MitoQ (in the form of MS010, MitoQ mesylate adsorbed to β-cyclodextrin) in drinking water was provided to wild type (WT) and Sca1$^{154Q/2Q}$ mice ad libitum for either 16 weeks (long term treatment; P40-P150) or for 3 weeks (short term treatment; P90-P110), whereas control mice were supplied with drinking water alone. Fresh MitoQ solution was applied twice a week.

Chromium treatment

Oxidative stress in mouse brain was induced as previously described (Travacio et al., 2000). In short, 25 mg/kg per day potassium dichromate (Chromium(VI); Merck) was applied in drinking water for 3 days.

Laser-Capture Microdissection (LCM) and Mass spectrometry (MS) analysis

LCM was performed as previously described (Ruegsegger et al., 2016). Mice were sacrificed by cervical dislocation. Cerebella were removed, embedded in O.C.T compound (Tissue TEK) and frozen on dry ice. 15 μm thick sections were cut by a cryostat, transferred onto membrane slides (membrane Slide 1.0 PET, Zeiss) and kept at -80°C. Prior to LCM, slides were thawed, stained

with Toluidine blue (0.1% Toluidine blue in PBS), rinsed in 70% and 100% ethanol (ETOH) and dried at room temperature (RT). LCM was performed using the PALM microBeam system (Zeiss). Areas of 3'000'000 μm^2 for PCs and 2'000'000 μm^2 for GCs were collected and moved into capture tube caps (AdhesiveCap 500 opaque, Zeiss). Proteins were extracted in 10 µl RIPA buffer after cell lysis. Tubes were centrifuged for 10 min at 16'000 x g (4°C) and stored at -80°C until MS.

MS was performed as previously described (Ruegsegger et al., 2016). Samples were loaded on a 12% SDS-gel and run to a distance of 1 cm. After staining the gel for 2 h in InstantBlue (Expedeon), lanes were cut into 10 bands, and each band into 4 pieces. Pieces were destained for 20 min in 30% ETOH, 30 min in 100% ETOH and washed 30 min in ddH_2O (cycle repeated thrice). Shotgun LCMS/MS was performed at the MS and Proteomics Core Facility of the Department of Clinical Research, University of Bern. Samples were measured 3x using a spectrum sampling approach and the MaxQuant software was used to assess the protein abundance (Heller et al., 2007). Only proteins with at least 3 or more unique peptides, having a PMSS higher than 30 and showing 2-fold changes were used for analysis.

Immunohistochemistry (IHC)

Mice were injected with 6 mg/kg anesthesia solution (24% Ketasol (Graeub), 16% Xylasol (Graeub), 60% NaCl solution 0.9% (Merck)) and intracardially perfused with 4% paraformaldehyde (PFA) in 0.1M PBS, pH = 7.4. Isolated cerebella were post-fixed overnight in 4% PFA and soaked for at least 24 h in 30% sucrose (in PBS, pH = 7.4). Sagittal 50 µm thick sections were cut with a cryostat and stored in 0.8% sodium-azide solution (in PBS, pH = 7.4). Sections were blocked in buffered 3% bovine serum albumin (BSA; Roche) for 2 h at RT followed by incubation in primary antibody (AB) solution (appropriate ABs, 3% BSA, 0.3% Triton X-100 in PBS, pH = 7.4) at 4°C for 2 days on a shaker. Section were washed 3x 30 min in washing solution (0.1% Triton X-100 in PBS, pH = 7.4) and incubated in secondary AB solution (appropriate ABs, 3% BSA, 0.3% Triton X-100 in PBS, pH = 7.4) over night at 4°C or 6 h at RT respectively. Section were washed again 3x 20 min in washing solution before they were mounted and coverslipped using mowiol mounting media. Following dilutions of antibodies were used: mouse anti-Calbindin, 1:1000 (ab82812, Abcam), rabbit anti-Calbindin, 1:1000 (ab11426, Abcam), mouse anti-8-hydroxy-guanosine (8-OHdG), 1:500 (ab62623, Abcam), goat anti-HSP60, 1:500 (sc-1052, Santa Cruz Biotechnology), secondary AB - Alexa Fluor conjugate, 1:1000 (Invitrogen). IHC using the goat anti-HSP60 AB required antigen retrieval prior to the blocking step. Sections were incubated for 20 min at 85°C in sodium citrate buffer (10 mM

dehydrate tri-sodium citrate (Merck), 0.05% Tween 20 (Merck) in ddH_2O, pH 6.0) and washed 2x 5 min in PBS.

Confocal Microscopy and Image analysis

All images were taken from lobule IX or at the primary fissure (only for PC cell number counting) with a confocal laser-scanning microscope Leica TCS SP8 (Leica Microsystem) or an Olympus Fluoview 1000-BX61 (Olympus, Tokyo).

Mitochondrial morphology analysis was assessed with 3D image analysis software Imaris 7.6 (Bitplane): Isosurfaces were generated for HSP60 intensities selectively within PC somas. Sphericity values of isosurfaces were exported for subsequent analysis. (1) Pooled data was plotted as histogram in order to display the distribution of mitochondria according to their shape. (2) Percentages of mitochondria falling below or above a reference value (median sphericity from age-matched WT control mice) were measured and used for statistical analysis. 8-OHdG intensities within PC somas (excluding nucleus) were measured using Fiji software. PC number was quantified in lobule V at the primary fissure over a distance of 315 µm as previously described (Ruegsegger et al., 2016). The plot profile of Fiji was used to quantify the Calbindin fluorescence intensity profile from the perikaryon center over the molecular layer as previously described (Watase et al., 2002). The profiles of different sections of age-matched mice were averaged and plotted.

Electron microscopy analysis

Anesthetized mice were intracardially perfused first with 0.1 M PBS (pH = 7.4) for 1 min and then fixed for 25 min with fixation solution (2.5% glutaraldehyde (GA) + 2% PFA in 0.1 M Na-cacodylate, pH = 7.4) at a speed of 8 ml/min. Cerebella were isolated 2 h after perfusion and post-fixed overnight at 4°C in fixation solution. 180 µm sagittal sections were cut with a vibratome. Bloc staining, dehydration and embedding were performed as previously described (Deerinck et al., 2010) with following modification: post-fixation was done in 0.15 M cacodylate buffer, 1.5% potassium ferrocyanide and 2% osmium tetroxide. Sample blocs were mounted on aluminium specimen pins (Gatan, Pleasonton, CA, USA) with a conductive silver epoxy glue. After a minimum of drying time of 4 h the blocs were imaged at the SBF-SEM using a Quanta FEG 250 (FEI, Eindhoven, The Netherlands), equipped with a Gatan 3View2XP in-situ ultramicrotome (Gatan). Images were recorded at 3.5 kV accelerating voltage in high vacuum. Pixel size was set to 12 nm and the slice thickness was set to values between 50 and 100 nm. Image rendering was done in UCSF Chimera (Pettersen et al., 2004) and mitochondrial length analysis in IMOD (Kremer et al., 1996).

Colorimetric measurements of ETC complexes: I, II, IV and V activities

Mice were sacrificed and cerebella were removed, embedded in O.C.T compound and frozen on dry ice. 14 µm thick, serial sections were cut by a cryostat and transferred onto an adhesive glass slide (LLG Labware). Sections were incubated for 40 min at 37°C in freshly prepared appropriate complex histochemistry media: (1) Complex I: 1.23 mg/ml (1.5 mM) Nitroblue tetrazolium (NBT; N6876, Sigma) and 0.625 mg/ml NADH (N8129, Sigma) were mixed in PBS, pH = 7.4 (adapted from (De Paepe et al., 2009). (2) Complex II: 1.23 mg/ml (1.5 mM) NBT, 35.12 mg/ml (130 mM) sodium succinate (S2378, Sigma), 0.0613 mg/ml (0.2 mM) Phenazine methosulfate (PMS; P9625, Sigma) and 0.065 mg/ml (1 mM) sodium azide (S8032, Sigma) were mixed in PBS (adapted from (Ross, 2011)). (3) Complex IV: 0.5 mg/ml 3,3'-diaminobenzidine Tetrahydrochloride (DAB; D7304, Sigma), 1 mg/ml cytochrome c (C2506, Sigma) and approximately 2 µg/ml (a few crystals) bovine catalase (C9322, Sigma) were mixed in PBS, pH = 7.4 (adapted from (Ross, 2011)). (4) A total of 100 ml complex V staining media contained 50 mg ATP (A2383, Sigma), 35.2 mg 2,4-dinitrophenol (D198501, Sigma), 40 ml 0.2 M Tris maleate buffer (0.2 M Tris Base, 0.2 M Maleic acid (M1296, Sigma), pH = 7.4), 6 ml 0.06 M lead nitrate (11520, Sigma), 10 ml 0.05 M magnesium chloride (Merck) and 44 ml ddH_2O. Following the incubation in complex V media, sections were washed 2x in PBS and incubated for 1 min at RT in 1% ammonium sulfide (adapted from (Karnes et al., 2010)). Subsequent to the staining of each complex, sections were washed 3x 10 min in PBS before they were dehydrated for 4 min in 70% ETOH, 4 min in 96% ETOH, 10 min in 100% ETOH and 10 min in Xylol and immediately mounted with Eukitt. 100x images were acquired with Nikon Eclipse E600 microscope using an Axiocam MRc 5 camera (Zeiss). Fiji software was used to measure intensity within PC soma.

Behavior assays

Motor coordination was assessed during the afternoon (2 - 6 pm) using a rotarod apparatus (Ugo Basile Biological Research Apparatus, Varese, Italy). The rotating speed was linearly increasing from 4 to 40 rpm in 300 s intervals. Mice were tested from P40-P150 once per week and scored for their latency to fall (in seconds). Each animal had to perform 4 trials per testing day with breaks of at least 10 min in between. The mean of the best 3 trials (per animal) was calculated and used for further analysis.

Hind limb clasping procedure was adapted from (Gennarino et al., 2015). Mice were clinched at the base of the tail and lifted away from objects for maximal 30 s. Hind limb positions were scored as follow: "0" if the hind limbs were totally opened away from the abdomen, "1" if only one hind limb was retracted close to the abdomen for more than 10 s, "2" if both hind limbs were

retracted close to the abdomen for more than 10 s, “3” if both hind limbs were more than 80% retracted and nearly touched the abdomen and “4” if both hind limbs were fully retracted and touched the abdomen.

Statistical Analysis

At least 3 biological replicates of every age-matched group were used for statistical analysis. Statistical significance was calculated with GraphPadPrism 5 and values are presented as mean ± standard error of the mean (SEM) or as box and whiskers (Turkey).

Results

PC specific proteome analysis reveals mitochondrial alterations at symptomatic stage of disease

Here, we focused on identifying PC specific cellular processes which would be altered at the symptomatic stage of disease and could contribute to the progression of the disease. As we have described previously (Ruegsegger et al., 2016), we laser dissected groups of PCs from the most affected cerebellar lobules VIII-X from P100, WT and Sca1$^{154Q/2Q}$ mice and analyzed the PC proteome by mass spectrometry. In a first set of experiments nearly 400 proteins were detected and shared between both genotypes. Only proteins with a minimum PMSS (Protein Match Score Summation) of 30 and for which 3 or more unique peptides had been identified, were taken as validly expressed. Of the 366 proteins reliably detected from two separate experiments, nearly 41% of the proteins displayed consistent alterations in expression levels in Sca1$^{154Q/2Q}$ PCs (**Fig. 1A**). This semi-quantitative analysis based on Protein Match Summation Score (PMSS) revealed an altered proteome; 27 proteins were upregulated and 124 were downregulated by at least two-fold. PANTHER (Protein ANalysis THrough Evolutionary Relationships) revealed an over-representation of altered proteins belonging to diverse cellular pathways and classes such as ATP synthesis, synaptic vesicle trafficking and glycolysis (**Fig. 1B**). Interestingly, 33% of the mutant PC proteome was down-regulated and protein classes such as oxidoreductases and nucleic acid binding were significantly overrepresented (**Fig. 1C**).

In particular, the majority of detected proteins involved in ATP synthesis and oxidoreductase activity were reduced in expression in Sca1$^{154Q/2Q}$ PCs. These included cytochrome c, ATP synthase subunit beta and ATP synthase subunit alpha (**Fig. 1D**). Additionally, several mitochondrial enzymes possessing oxidoreductase activity such as thioredoxin-dependent peroxide reductase, mitochondrial cytochrome c oxidase subunit 5A, mitochondrial NADH

dehydrogenase [ubiquinone] 1 alpha subcomplex subunit 13, NADH dehydrogenase [ubiquinone] flavoprotein 2, mitochondrial cytochrome b-c1 complex subunit 6, mitochondrial cytochrome c oxidase subunit 6B1 were significantly reduced in the Sca1$^{154Q/2Q}$ PC cells (**Fig. 1E**). The extensive mitochondria-specific proteome alterations hinted towards impairment of mitochondrial function. Moreover, we had identified previously that at an early presymptomatic stage, around 4 weeks after birth, mutant PCs exhibited significant overrepresentation for alterations associated with synaptic and calcium binding protein classes, but not with mitochondrial proteins (Ruegsegger et al., 2016). In view of those findings, the detection of significant alterations in mitochondria-associated proteins at later symptomatic stages of disease, suggested that mitochondrial alterations might appear gradually, coinciding with the symptomatic phase of the disease and synergistically contribute to disease progression. For the complete list of altered proteins see **Table S1**.

Age-dependent alterations in mitochondrial morphology in Sca1$^{154Q/2Q}$ mice

Based on the proteomic data at P100, we next examined whether mitochondria themselves exhibited age-dependent alterations in mutant PCs. Using HSP60 as a mitochondrial marker, immunostaining of cerebellar sections at various ages revealed that HSP60 immunopositive mitochondria appeared more vesicular and condensed with increasing age in Calbindin positive PCs of Sca1$^{154Q/2Q}$ mice (**Fig. 2A**). Interestingly, at P60 mutant PCs exhibited a nearly normal mitochondrial morphology compared to those observed in the WT mice, however from P110 onwards, Sca1$^{154Q/2Q}$ PCs presented visible and sustained alterations in mitochondrial morphology. In order to obtain a quantitative measure for the observed changes in mitochondrial shape, we generated 3D-isosurface for individual mitochondria within PCs and measured their sphericity (**Suppl. Fig. 1**). A histogram plotted for sphericity, where larger values, closer to 1.0, indicate a more spherical or vesicular structure, whereas smaller values indicate a more tubular structure, revealed that P110 WT mitochondria were enriched for smaller values as compared to mutant mitochondria. Notably, P110 Sca1$^{154Q/2Q}$ mitochondria distributed in higher numbers towards values closer to 1.0 compared to WT, suggesting that as the disease progressed the mitochondria acquired an altered, more vesicular morphology. To obtain quantitative significance for the observed differences, the percentage of mitochondria falling below (tubular) or above (vesicular) a critical sphericity value (i.e. the median value for the WT mice) were measured at three different ages; P60, P110 and P150. While in WT mice the ratio between tubular versus vesicular mitochondria was 50% at all ages, these ratios were significantly altered in Sca1$^{154Q/2Q}$ PCs. These analyses confirmed that a proportion of mitochondria in mutant PCs from P110 onwards were morphologically altered and were more vesicular in shape (**Fig. 2B**).

Subsequently, ultrastructural analysis of mitochondria in PCs was performed by serial block-face scanning electron microscopy (SBF-SEM) and 3D-reconstruction of the images (**Fig. 2C**). The sketch indicates a representative spread of mitochondria in WT and mutant PCs. Note the presence of more tubular interlinked and elongated mitochondria in WT and the rather sparse, fragmented and short mitochondria present in mutant P150 Sca1$^{154Q/2Q}$ PCs. Measurement of the mitochondrial length in individual PCs further confirmed that in mutant PCs shorter mitochondria were dominant. Quantitative analysis demonstrated that 69% of mitochondria in Sca1$^{154Q/2Q}$ PCs fall below the median length of the WT mitochondria. Moreover, nearly 48% of mitochondria ranged in length from 1-1499 nm in mutant PCs, whereas in WT this was about 31%, demonstrating that mutant PCs have altered mitochondrial morphology (**Fig. 2D**).

Electron transport chain (ETC) deficits in mitochondria parallel changes in mitochondrial morphology in Sca1$^{154Q/2Q}$ PCs

After having established that morphological impairment to mitochondria appear at around the same time as the disease symptoms, but are absent at earlier ages, we next examined whether these alterations correlated with a deficit in mitochondrial function. Since, the primary function of mitochondria is energy production in the form of an elevated ATP/ADP ratio, we focused on assessing whether deficits in ETC function and ATP production were observed in mutant PCs. To this end, we used a colorimetric assay to assess Complex I, II, IV and V activity in WT and Sca1$^{154Q/2Q}$ PCs. Complex I activity was measured via the NADH dehydrogenase catalysed redox reaction in which NADH was oxidized and nitroblue tetrazolium (NBT) was reduced. The blue colour so formed due to NBT reduction directly correlates with the amount of endogenous NADH dehydrogenase activity present within PCs and was specifically and significantly reduced at P110 in Sca1$^{154Q/2Q}$ PCs as compared to WT PCs (**Fig. 3A**). Interestingly, areas outside the PCs such as the granule cell layer (GL) and molecular layer (ML) did not display any differences in the NBT intensity, suggesting that Complex I activity reduction was restricted to regions-associated with disease vulnerable PCs. Similarly, measurement of Complex II activity via succinate dehydrogenase revealed a statistically significant decline in activity in Sca1$^{154Q/2Q}$ PCs (**Fig. 3B**). Subsequently, we analyzed the activity of Complex IV by measuring the intensity of cytochrome c oxidation, which is detected by the brown coloring produced by the oxidation of diaminobenzidine (DAB), and also found reduced Complex IV activity in P110 in Sca1$^{154Q/2Q}$ PCs compared to WT PCs (**Fig. 3C**). Lastly, we measured mitochondrial ATP synthase activity by complex V. This enzyme consumes energy stored in the proton electrochemical potential gradient across the membrane to generate ATP from ADP and phosphate. The resultant brown coloring due to formation of brown lead sulfide from ammonium sulfide in the colorimetric

reaction quantitatively correlates with mitochondrial ATP synthase activity. As with previous observations Complex V levels were diminished in mutant PCs providing evidence for reduced ATP production. Taken together, these experiments demonstrated that ETC complex activity as well as ATP production is impaired in Sca1$^{154Q/2Q}$ PCs at symptoms (**Fig. 3D**).

Symptomatic appearance of oxidative stress induced DNA damage coincides with mitochondrial deficits

As mitochondria contributes to many cellular processes such as ATP synthesis, ROS production, synaptic transmission, calcium homeostasis, and apoptosis, the compromised physiological function of mitochondria in Sca1$^{154Q/2Q}$ PCs would adversely affect those critical processes. The gradual appearance of mitochondrial dysfunction in Sca1$^{154Q/2Q}$ PCs at the stage when symptoms become evident hinted that a mitochondria-specific stressor might be involved in the observed impairment, therefore we focused on oxidative stress as a likely form of damage. Firstly, we verified whether chromium-induced oxidative stress leads to morphological alterations in WT PCs. A three day chromium treatment regime was performed at P110, an age where in the mutant condition mitochondrial changes are observed. This treatment led to the appearance of vesicular- shaped and fragmented mitochondria in WT PCs, suggesting that oxidative stress might also alter mitochondrial morphology in the disease model (**Fig. 4A**). To further confirm that the appearance of oxidative stress at a particular stage in disease correlates with the functional mitochondrial alterations, we measured ETC complexes in WT mice after three day chromium treatment regime. This treatment led to a conspicuous reduction in the activity of Complexes I and IV, thereby mimicking the impairments observed in mutant PCs (**Fig. 4B**).

As oxidative stress induces DNA damage including mitochondrial DNA damage, an antibody against the oxidative DNA damage biomarker; 8-hydroxy-2'-deoxyguanosine (8-OHdG) was applied to cerebellar sections from both genotypes at P60 (early symptomatic stage), P110 (symptomatic stage) and P150 (late symptomatic stage) of disease. At P60, low and equal amounts of immunoreactivity of 8-OHdG was observed in both genotypes (**Fig. 4C**). However, by P110, enhanced 8-OHdG immunoreactivity was observed selectively in Sca1$^{154Q/2Q}$ PCs, whereas in WT PCs 8-OHdG immunoreactivity remained nearly unchanged from that measured at P60. At P150, the intensity of 8-OHdG immunolabeling was significantly increased in Sca1$^{154Q/2Q}$ PCs, indicating that oxidative stress induced DNA damage was present in mutant PCs at symptomatic stages (**Fig. 4D**). Altered mitochondrial morphology associated with oxidative stress and the corresponding evidence for DNA damage in mutant PCs at P110 but not

at P60 further strengthened our observation that mitochondrial impairments appear gradually during the symptomatic stage of the disease and are absent at early presymptomatic stages.

Administration of the mitochondria-targeted antioxidant MitoQ improves mitochondrial morphology

Our observation that the appearance of enhanced oxidative stress correlates with impaired mitochondrial morphology and functioning raised the question whether reduction in oxidative damage might improve observed mitochondrial deficits present specifically within Sca1$^{154Q/2Q}$ PCs. To this end, we decided to treat mice with MitoQ (mitoquinone mesylate: [10-(4,5-dimethoxy-2-methyl-3,6-dioxo-1,4-cycloheexadienlyl) decyl triphenylphosphonium methanesulfonate]), which is a mitochondria-targeted antioxidant that specifically accumulates within the mitochondria in vivo and moreover, no deleterious side effects or pro-oxidative properties have been found after long term treatment with the levels of MitoQ we use (Rodriguez-Cuenca et al., 2010). Firstly, we started the administration of MitoQ at P40, an early age before mitochondrial changes are observed. The treatment was continued until P150, an age corresponding to a late stage of the disease, where mitochondrial impairments are present in Sca1$^{154Q/2Q}$ PCs. Examining mitochondrial morphology at P150 revealed that WT mice did not show any significant alterations after MitoQ, treatment, although there was a trend towards a slight increase in the ratio between tubular mitochondria versus vesicular mitochondria. Notably, MitoQ administration to Sca1$^{154Q/2Q}$ mice for more than hundred days significantly delayed the appearance of alterations in mitochondrial morphology and the ratio between tubular and vesicular mitochondria remained closer to those observed in WT conditions **(Fig. 5A-B**).

Subsequently, we administered MitoQ at ages when morphological alterations to mitochondria were already present in order to examine whether MitoQ could now ameliorate existing alterations. Short-term MitoQ treatment from P90 to P110 in Sca1$^{154Q/2Q}$ mice was sufficient to reduce the percentage of vesicular shaped mitochondria to amounts similar to those observed in WT PCs (**Fig. 5C-D**), demonstrating that oxidative stress is involved in symptomatic mitochondria-associated alterations in SCA1. Lastly, we performed an ultrastructural analysis of mitochondria in PCs by serial block-face scanning electron microscopy (SBF-SEM) and 3D-reconstruction of the images. Here, we treated mice with MitoQ from P90 to P110 and the length of the reconstructed mitochondria was measured. As previously observed via immunohistochemistry, ultrastructural analysis also revealed a shift in the distribution of Sca1$^{154Q/2Q}$ mitochondria from shorter to longer lengths after MitoQ treatment, suggestive of a correlation between levels of oxidative stress and mitochondrial morphology (**Fig. 5E-F**).

MitoQ treatment restores mitochondrial function in Sca1$^{154Q/2Q}$ PCs

Next, we examined whether MitoQ treatment would have the potential to completely inhibit or slow down the deficits in ETC and ATP production which were observed in mutant PCs. After chronically treating mutant and WT mice with MitoQ (P40-P150), we assessed the activity of Complexes I, II, IV and V in WT and Sca1$^{154Q/2Q}$ PCs. Complex I activity revealed that in MitoQ treated Sca1$^{154Q/2Q}$ PCs, this activity was restored to similar levels as those observed in WT condition. While significant reduction in Complex I activity was observed between WT and Sca1$^{154Q/2Q}$ PCs at P150, no difference was observed between P150, WT and MitoQ treated Sca1$^{154Q/2Q}$ PCs, indicating that the antioxidant MitoQ was effective in inhibiting or delaying ETC complex impairments (**Fig. 6A**). Similarly, measurement of the Complex II activity via succinate dehydrogenase revealed a statistically significant increase in activity in MitoQ treated Sca1$^{154Q/2Q}$ PCs (**Fig. 6B**). We further analyzed the activity of Complex IV and as with the other complexes of the ETC found near normal levels of Complex IV activity in MitoQ treated Sca1$^{154Q/2Q}$ PCs (**Fig. 6C**). Finally, we measured mitochondrial ATP synthase activity and yet again found normal levels of Complex V activity in MitoQ treated mutant PCs (**Fig. 6D**).

In these experiments Sca1$^{154Q/2Q}$ mice were chronically treated with MitoQ from an early symptomatic stage, therefore we next specifically evaluated whether a short MitoQ treatment in mutant mice at a stage, when mitochondrial impairments are already present, would have a beneficial effect. Treating mice with MitoQ for twenty days from p90-P110 revealed that all ETC complex activities were restored to near WT levels (**Suppl. Fig. 2A-D**). Moreover, 8-OHdG immunoreactivity was restored to WT levels in Sca1$^{154Q/2Q}$ PCs (**Suppl. Fig. 2E**), indicating that even short duration of MitoQ treatment after symptoms were established was sufficient to restore mitochondrial functioning.

MitoQ administration ameliorates SCA1-associated pathology in Sca1$^{154Q/2Q}$ mice

We next assessed whether the amelioration in mitochondrial morphology and functionality by MitoQ could also positively impact SCA1-linked pathological features such as impaired motor coordination, gait imbalance and hind-limb clasping. Notably, while Sca1$^{154Q/2Q}$ mice from P50 onwards, exhibited a gradual decline in rotarod performance, MitoQ treated Sca1$^{154Q/2Q}$ mice remained consistently stable from P90 onwards. With increasing age the performance of Sca1$^{154Q/2Q}$ mice on the rotarod significantly diminished compared to those of MitoQ treated Sca1$^{154Q/2Q}$ mice, which remained consistently stable and significantly higher compared to the mutant mice at all stages of the disease (**Fig. 7A**). Interestingly, WT MitoQ treated mice also exhibited a slight improvement in motor coordination as compared to untreated WT control mice

(**Fig. 7A**). Furthermore, clasping of hind-limbs was significantly reduced in Sca1$^{154Q/2Q}$ MitoQ treated mice compared to untreated littermates and this was already visible after 70 days of MitoQ treatment (**Fig. 7B)**.

Additionally, we examined the impact of MitoQ treatment on SCA1-associated cellular alterations such as decline in Calbindin expression levels correlating with the degeneration of PC spines and the loss of PCs. Measurement of expression intensities for Calbindin from the perikaryon center along the dendrites revealed that PCs from P150 Sca1$^{154Q/2Q}$ mice which had been treated with MitoQ from P40 onwards had higher Calbindin expression levels than PCs from untreated Sca1$^{154Q/2Q}$ mice of the same age, indicative of sustained PC functioning (**Fig. 7C**). Calbindin labeling intensities were slightly higher in PCs from Sca1$^{154Q/2Q}$ at P110, where MitoQ treatment had been initiated after mitochondrial impairments were evident and only for a short duration of 20 days (**Fig. 7C**). Subsequently, counting of PCs at P150 after chronic MitoQ treatment revealed unchanged PC numbers in MitoQ treated mutant PCs compared to WT mice, whereas reduced PC numbers, suggestive of PC degeneration, were observed in Sca1$^{154Q/2Q}$ cerebellum (**Fig. 7D**). A similar positive effect of MitoQ on PC numbers was also observed at P110 when the mice had been treated with MitoQ for a short period of time, highlighting the potential of MitoQ to not only prevent but also ameliorate disease-associated cellular impairments.

Discussion

This study was initiated to identify SCA1-associated alterations that would influence disease progression and related symptoms. To this end, we performed a PC-specific proteome analysis of mutant Sca1$^{154Q/2Q}$ mice at P100, when symptoms are evident. This approach revealed an accumulation of mitochondrial alterations in mutant PCs compared to WT. Interestingly, in our previous study using similar approaches at presymptomatic stages, we identified significant enrichment for synaptic alterations in mutant PCs immediately after cerebellar maturation. Moreover, expression changes in the synaptic proteome involving the PC spine specific protein Homer-3 and also impaired glutamatergic signaling were implicated in the pathophysiology of SCA1 by us and by others (Ingram et al., 2016; Ruegsegger et al., 2016; Serra et al., 2004). Therefore, the appearance of significant deficits in mitochondria-associated proteins at an age coinciding with the onset of symptoms suggested that in addition to early synaptic deficits, mitochondrial impairments are also important contributors to the progression of SCA1. To further understand the significance of these mitochondrial alterations to SCA1 pathology, we specifically

examined mitochondrial morphology and function, which revealed an age-dependent morphological and functional impairment in the activities of the mitochondrial ETC and ATPase complexes that was associated with oxidative damage.

There is considerable evidence linking mitochondrial dysfunction, impaired energy metabolism and oxidative stress to the pathophysiology of NDs (Lin and Beal, 2006). Deficits in mitochondrial function have been strongly implicated in ALS, AD, PD, HD, hereditary spastic paraplegia, Friedreich's ataxia, and Charcot-Marie-Tooth disease (Allen et al., 2015; DiMauro and Schon, 2008; Ruffoli et al., 2015; Tatsuta and Langer, 2008). Besides the involvement of mitochondria in neuronal development and energy production, mitochondria are also involved in a plethora of essential neuron specific processes such as calcium homeostasis, maintenance of membrane potential, axonal and dendritic transport, and the release, uptake and reuse of neurotransmitters in the synapses. In the context of PolyQ disorders, studies on HD animal and cultured cell models have linked defective mitochondrial bioenergetics to HD pathogenesis. In HD patients, reductions in the activities of the mitochondrial ETC complexes II, III and IV have been observed in the postmortem brain (Brennan et al., 1985; Browne et al., 1997; Gu et al., 1996). Similar observations involving dysfunctional respiratory chain complexes and increased oxidative stress has been made in the pathology associated with the SCA2, SCA3, and SCA12 forms of spastic paraplegia (Simon et al., 2007; Wang et al., 2011; Yu et al., 2009). In the case of SCA1, mutant ATXN1 was shown to bind and impair the function of HMGB1, a DNA damage repair protein which was also implicated in mitochondrial DNA damage repair, thereby indirectly linking mitochondrial DNA damage to SCA1 disease progression (Ito et al., 2015). Consistent with this observation, we found a significant increase in the oxidative DNA damage biomarker; 8-OHdG in an age-dependent manner, coinciding with the symptomatic phase of the disease. Further, we found considerable reduction in activities of ETC complexes paralleling the appearance of increased 8-OHdG immunoreactivity, suggesting that oxidative damage to the mitochondrial DNA might affect the transcription of critical mitochondrial proteins or that the damage occurs directly to the proteins. In this regard, our proteomic screen also revealed that a significant number of mitochondrial proteins involved in the ETC complexes and the ATP synthase were downregulated in mutant PCs, thereby affecting bioenergetics and proper mitochondrial functioning. Additionally, it is well accepted that calcium signaling is impaired in SCA1, SCA2 and SCA3 (Brown and Loew, 2012; Halbach et al., 2016; Kasumu et al., 2012; Pellistri et al., 2013) and as mitochondria are the second most important calcium storage organelle, improper mitochondrial functioning can negatively impact calcium homeostasis and neuronal transmission (Wang et al., 2015).

As ETC activity governs the synthesis of ATP, deficits in ETC complexes would inevitably affect those metabolic processes that require energy. Metabolic deficits and the loss of body weight at early stages of the disease are the most common symptoms observed in SCA1 patients (Mahler et al., 2014) as well as in SCA1 mouse models (Jafar-Nejad et al., 2011; Watase et al., 2002). Another striking feature of metabolic alteration specifically observed in the cerebellum and brain stem of SCA1 patients is a decline in total NAA (N-acetylaspartate + N-acetylglutamate levels with a concomitant increase in total levels of creatine, myoinositol and glutamine. This reduction in total NAA levels directly correlates with SCA1 patients' ataxia scores and similar changes have also been observed in SCA1 mouse models. Notably, these changes have been demonstrated to be dependent on the expression of mutant ATXN1 protein and its deletion in conditional SCA1 models rescues those deficits (Emir et al., 2013; Guerrini et al., 2004; Oz et al., 2010). Interestingly, N-acetylaspartate (NAA) is synthesized by mitochondria and is a neuron-specific metabolite. The reduction in NAA levels is a direct indicator of disturbances in ATP production, neuronal injury and compromised neuronal viability (Moffett et al., 2013; Signoretti et al., 2008). Moreover, the relationship of mitochondrial NAA synthesis with oxygen consumption and ATP production hints at reduced NAA levels in SCA1 patients and mouse models as reflecting suboptimal mitochondrial energy production. In this regard our finding that mutant $Sca1^{154Q/2Q}$ PCs exhibit mitochondrial dysfunction, mainly involving reduced activities of ETC complexes, provides a framework for accounting for the previously observed changes in total NAA levels as being due to impaired energy production in mutant PCs.

Over the past few years, mitochondria have become a therapeutic target in NDs and one potential therapeutic agent is MitoQ. It consists of a ubiquinone moiety linked to a positively charged lipophilic cation that allows its selective and extensive accumulation within mitochondria driven by the high mitochondrial membrane potential (Smith and Murphy, 2010). Within mitochondria, the ubiquinone moiety is rapidly reduced to the active antioxidant form ubiquinol by respiratory complex II (James et al., 2007). The protective effect of MitoQ against oxidative stress has been shown in a number of neurodegenerative mouse models such as for ALS (Miquel et al., 2014), AD (McManus et al., 2011) and PD (Ghosh et al., 2010). Therefore, we examined whether MitoQ administration would be beneficial in improving mitochondrial deficits and preventing ataxia-like pathology in mouse model of SCA1. MitoQ treatment reversed mitochondrial morphological alterations and restored activities of ETC complexes. To examine whether the mitochondrial protection conferred by MitoQ was sufficient to prevent the emergence of SCA1 pathology in vivo, we treated young $Sca1^{154Q/2Q}$ mice, which do not exhibit mitochondrial deficits with MitoQ for 110 days and evaluated the effect on the appearance of SCA1-associated symptoms. Notably, MitoQ treatment slowed down the development of motor

incoordination and the appearance of gait deficits. Moreover, MitoQ administration significantly reduced PC dendrite and PC degeneration. Remarkably, treatment of Sca1$^{154Q/2Q}$ mice with MitoQ for short periods of time when mitochondrial impairments and behavioral deficits were already present, revealed a substantial improvement of mitochondrial function and reduced PC loss. This short treatment regime of MitoQ is clinically feasible and, as MitoQ has been given to PD patients safely for up to a year (Snow et al., 2010), could be administered to patients after their diagnosis with SCA1.

The precise pathways which lead to the observed deficits in mitochondrial bioenergetics remain uncertain, however, it is likely that mutant ATXN1 could negatively influence the transcription of multiple genes encoding important mitochondrial proteins, which in turn impair critical oxidative and energy-associated metabolic pathways. Moreover, higher ROS levels and mutant ATXN1-linked reduction of the high-mobility group box 1 protein (HMGB1) in mitochondria could lead to accumulation of mitochondrial DNA damage, which might synergistically contribute to suboptimal mitochondrial functioning. Further, our previous study had implicated early synaptic deficits involving the reduced expression of calcium binding proteins and PC spine-specific protein Homer-3 in regulating SCA1 pathophysiology (Ruegsegger et al., 2016). Early impairment in PC specific calcium homeostasis could lead to a mitochondrial calcium overload. It has been previously shown that mitochondrial calcium overload causes mitochondrial fragmentation and oxidative stress (Peng and Jou, 2010). In this regard, it will be interesting in the future to examine whether synaptic deficits and impaired calcium homeostasis also influences mitochondrial functioning or whether these cellular dysfunctions are independent events in SCA1. Taken together, our work reveals an important role for mitochondria dysfunction in SCA1 progression and provides evidence for the beneficial use of the mitochondria-targeted antioxidant MitoQ in SCA1.

Author Contributions

S.S. and D.M.S. conceived the study, D.M.S., C.R., and S.St. performed experiments and analyses. J.R., B.Z. performed SBF-SEM, and M.P.M. provided MitoQ reagent and technical advice. S.S. directed and supervised the overall project and wrote the manuscript.

Acknowledgements

We thank Ruth Rehmann for maintaining mouse colonies, Beat Haenni and Adolfo Odriozola for SBF-SEM tissue processing and assistance in SBF-SEM imaging. Manfred Heller from the Department of Clinical Research, University of Bern for Mass Spectrometry.

Funding

This work was supported by Swiss National Science Foundation Professorship grant # 150756 to S.S. which funded C.R. and D.M.S. Microscopy was performed on equipment supported by the Microscopy Imaging Center (MIC), University of Bern, Switzerland. M.P.M consults for, and holds shares in, Antipodean Inc which is commercializing MitoQ

References

Allen, S.P., Duffy, L.M., Shaw, P.J., and Grierson, A.J. (2015). Altered age-related changes in bioenergetic properties and mitochondrial morphology in fibroblasts from sporadic amyotrophic lateral sclerosis patients. Neurobiol Aging 36, 2893-2903.

Ayala-Pena, S. (2013). Role of oxidative DNA damage in mitochondrial dysfunction and Huntington's disease pathogenesis. Free Radic Biol Med 62, 102-110.

Beal, M.F. (1996). Mitochondria, free radicals, and neurodegeneration. Curr Opin Neurobiol 6, 661-666.

Brennan, W.A., Jr., Bird, E.D., and Aprille, J.R. (1985). Regional mitochondrial respiratory activity in Huntington's disease brain. J Neurochem 44, 1948-1950.

Brown, S.A., and Loew, L.M. (2012). Computational analysis of calcium signaling and membrane electrophysiology in cerebellar Purkinje neurons associated with ataxia. BMC Syst Biol 6, 70.

Browne, S.E., Bowling, A.C., MacGarvey, U., Baik, M.J., Berger, S.C., Muqit, M.M., Bird, E.D., and Beal, M.F. (1997). Oxidative damage and metabolic dysfunction in Huntington's disease: selective vulnerability of the basal ganglia. Annals of neurology 41, 646-653.

Burk, K., Abele, M., Fetter, M., Dichgans, J., Skalej, M., Laccone, F., Didierjean, O., Brice, A., and Klockgether, T. (1996). Autosomal dominant cerebellar ataxia type I clinical features and MRI in families with SCA1, SCA2 and SCA3. Brain 119 (Pt 5), 1497-1505.

Burright, E.N., Clark, H.B., Servadio, A., Matilla, T., Feddersen, R.M., Yunis, W.S., Duvick, L.A., Zoghbi, H.Y., and Orr, H.T. (1995). SCA1 transgenic mice: a model for neurodegeneration caused by an expanded CAG trinucleotide repeat. Cell 82, 937-948.

Burte, F., Carelli, V., Chinnery, P.F., and Yu-Wai-Man, P. (2015). Disturbed mitochondrial dynamics and neurodegenerative disorders. Nat Rev Neurol 11, 11-24.

Calabrese, V., Lodi, R., Tonon, C., D'Agata, V., Sapienza, M., Scapagnini, G., Mangiameli, A., Pennisi, G., Stella, A.M., and Butterfield, D.A. (2005). Oxidative stress, mitochondrial dysfunction and cellular stress response in Friedreich's ataxia. J Neurol Sci 233, 145-162.

Calabrese, V., Scapagnini, G., Giuffrida Stella, A.M., Bates, T.E., and Clark, J.B. (2001). Mitochondrial involvement in brain function and dysfunction: relevance to aging, neurodegenerative disorders and longevity. Neurochem Res 26, 739-764.

Chaturvedi, R.K., and Flint Beal, M. (2013). Mitochondrial diseases of the brain. Free Radic Biol Med 63, 1-29.

Cozzolino, M., Ferri, A., Valle, C., and Carri, M.T. (2013). Mitochondria and ALS: implications from novel genes and pathways. Mol Cell Neurosci 55, 44-49.

Criscuolo, C., Procaccini, C., Meschini, M.C., Cianflone, A., Carbone, R., Doccini, S., Devos, D., Nesti, C., Vuillaume, I., Pellegrino, M., et al. (2015). Powerhouse failure and oxidative damage in autosomal recessive spastic ataxia of Charlevoix-Saguenay. J Neurol 262, 2755-2763.

De Paepe, B., De Bleecker, J.L., and Van Coster, R. (2009). Histochemical methods for the diagnosis of mitochondrial diseases. Curr Protoc Hum Genet Chapter 19, Unit19 12.

Deerinck, T.J., Bushong, E.A., Thor, A., and Ellisman, M.H. (2010). NCMIR methods for 3D EM: a new protocol for preparation of biological specimens for serial block face scanning electron microscopy. Microscopy, 6-8.

DiMauro, S., and Schon, E.A. (2008). Mitochondrial disorders in the nervous system. Annu Rev Neurosci 31, 91-123.

Duffy, L.M., Chapman, A.L., Shaw, P.J., and Grierson, A.J. (2011). Review: The role of mitochondria in the pathogenesis of amyotrophic lateral sclerosis. Neuropathol Appl Neurobiol 37, 336-352.

Emir, U.E., Brent Clark, H., Vollmers, M.L., Eberly, L.E., and Oz, G. (2013). Non-invasive detection of neurochemical changes prior to overt pathology in a mouse model of spinocerebellar ataxia type 1. J Neurochem 127, 660-668.

Fernandez-Funez, P., Nino-Rosales, M.L., de Gouyon, B., She, W.C., Luchak, J.M., Martinez, P., Turiegano, E., Benito, J., Capovilla, M., Skinner, P.J., et al. (2000). Identification of genes that modify ataxin-1-induced neurodegeneration. Nature 408, 101-106.

Friedland-Leuner, K., Stockburger, C., Denzer, I., Eckert, G.P., and Muller, W.E. (2014). Mitochondrial dysfunction: cause and consequence of Alzheimer's disease. Prog Mol Biol Transl Sci 127, 183-210.

Gennarino, V.A., Singh, R.K., White, J.J., De Maio, A., Han, K., Kim, J.Y., Jafar-Nejad, P., di Ronza, A., Kang, H., Sayegh, L.S., et al. (2015). Pumilio1 haploinsufficiency leads to SCA1-like neurodegeneration by increasing wild-type Ataxin1 levels. Cell 160, 1087-1098.

Ghosh, A., Chandran, K., Kalivendi, S.V., Joseph, J., Antholine, W.E., Hillard, C.J., Kanthasamy, A., Kanthasamy, A., and Kalyanaraman, B. (2010). Neuroprotection by a mitochondria-targeted drug in a Parkinson's disease model. Free Radic Biol Med 49, 1674-1684.

Girard, M., Lariviere, R., Parfitt, D.A., Deane, E.C., Gaudet, R., Nossova, N., Blondeau, F., Prenosil, G., Vermeulen, E.G., Duchen, M.R., et al. (2012). Mitochondrial dysfunction and Purkinje cell loss in autosomal recessive spastic ataxia of Charlevoix-Saguenay (ARSACS). Proc Natl Acad Sci U S A 109, 1661-1666.

Gu, M., Gash, M.T., Mann, V.M., Javoy-Agid, F., Cooper, J.M., and Schapira, A.H. (1996). Mitochondrial defect in Huntington's disease caudate nucleus. Annals of neurology 39, 385-389.

Guedes-Dias, P., Pinho, B.R., Soares, T.R., de Proenca, J., Duchen, M.R., and Oliveira, J.M. (2015). Mitochondrial dynamics and quality control in Huntington's disease. Neurobiol Dis.

Guerrini, L., Lolli, F., Ginestroni, A., Belli, G., Della Nave, R., Tessa, C., Foresti, S., Cosottini, M., Piacentini, S., Salvi, F., et al. (2004). Brainstem neurodegeneration correlates with clinical dysfunction in SCA1 but not in SCA2. A quantitative volumetric, diffusion and proton spectroscopy MR study. Brain 127, 1785-1795.

Haelterman, N.A., Yoon, W.H., Sandoval, H., Jaiswal, M., Shulman, J.M., and Bellen, H.J. (2014). A mitocentric view of Parkinson's disease. Annu Rev Neurosci 37, 137-159.

Halbach, M.V., Gispert, S., Stehning, T., Damrath, E., Walter, M., and Auburger, G. (2016). Atxn2 Knockout and CAG42-Knock-in Cerebellum Shows Similarly Dysregulated Expression in Calcium

Homeostasis Pathway. Cerebellum.

Hang, L., Thundyil, J., and Lim, K.L. (2015). Mitochondrial dysfunction and Parkinson disease: a Parkin-AMPK alliance in neuroprotection. Ann N Y Acad Sci 1350, 37-47.

Heller, M., Schlappritzi, E., Stalder, D., Nuoffer, J.M., and Haeberli, A. (2007). Compositional protein analysis of high density lipoproteins in hypercholesterolemia by shotgun LC-MS/MS and probabilistic peptide scoring. Mol Cell Proteomics 6, 1059-1072.

Ingram, M., Wozniak, E.A., Duvick, L., Yang, R., Bergmann, P., Carson, R., O'Callaghan, B., Zoghbi, H.Y., Henzler, C., and Orr, H.T. (2016). Cerebellar Transcriptome Profiles of ATXN1 Transgenic Mice Reveal SCA1 Disease Progression and Protection Pathways. Neuron 89, 1194-1207.

Ito, H., Fujita, K., Tagawa, K., Chen, X., Homma, H., Sasabe, T., Shimizu, J., Shimizu, S., Tamura, T., Muramatsu, S., et al. (2015). HMGB1 facilitates repair of mitochondrial DNA damage and extends the lifespan of mutant ataxin-1 knock-in mice. EMBO Mol Med 7, 78-101.

Jafar-Nejad, P., Ward, C.S., Richman, R., Orr, H.T., and Zoghbi, H.Y. (2011). Regional rescue of spinocerebellar ataxia type 1 phenotypes by 14-3-3epsilon haploinsufficiency in mice underscores complex pathogenicity in neurodegeneration. Proc Natl Acad Sci U S A 108, 2142-2147.

James, A.M., Sharpley, M.S., Manas, A.R., Frerman, F.E., Hirst, J., Smith, R.A., and Murphy, M.P. (2007). Interaction of the mitochondria-targeted antioxidant MitoQ with phospholipid bilayers and ubiquinone oxidoreductases. The Journal of biological chemistry 282, 14708-14718.

Karbowski, M., and Neutzner, A. (2012). Neurodegeneration as a consequence of failed mitochondrial maintenance. Acta Neuropathol 123, 157-171.

Karnes, H.E., Scaletty, P.N., and Durham, D. (2010). Histochemical and fluorescent analyses of mitochondrial integrity in chick auditory neurons following deafferentation. J Am Acad Audiol 21, 204-218.

Kasumu, A.W., Liang, X., Egorova, P., Vorontsova, D., and Bezprozvanny, I. (2012). Chronic suppression of inositol 1,4,5-triphosphate receptor-mediated calcium signaling in cerebellar purkinje cells alleviates pathological phenotype in spinocerebellar ataxia 2 mice. The Journal of neuroscience : the official journal of the Society for Neuroscience 32, 12786-12796.

Koeppen, A.H. (1991). The Purkinje cell and its afferents in human hereditary ataxia. J Neuropathol Exp Neurol 50, 505-514.

Kremer, J.R., Mastronarde, D.N., and McIntosh, J.R. (1996). Computer visualization of three-dimensional image data using IMOD. J Struct Biol 116, 71-76.

Labbadia, J., and Morimoto, R.I. (2013). Huntington's disease: underlying molecular mechanisms and emerging concepts. Trends Biochem Sci 38, 378-385.

Lin, M.T., and Beal, M.F. (2006). Mitochondrial dysfunction and oxidative stress in neurodegenerative diseases. Nature 443, 787-795.

Magrane, J., and Manfredi, G. (2009). Mitochondrial function, morphology, and axonal transport in amyotrophic lateral sclerosis. Antioxid Redox Signal 11, 1615-1626.

Mahler, A., Steiniger, J., Endres, M., Paul, F., Boschmann, M., and Doss, S. (2014). Increased catabolic state in spinocerebellar ataxia type 1 patients. Cerebellum 13, 440-446.

Manfredi, G., and Beal, M.F. (2000). The role of mitochondria in the pathogenesis of neurodegenerative diseases. Brain Pathol 10, 462-472.

McManus, M.J., Murphy, M.P., and Franklin, J.L. (2011). The mitochondria-targeted antioxidant MitoQ prevents loss of spatial memory retention and early neuropathology in a transgenic

mouse model of Alzheimer's disease. The Journal of neuroscience : the official journal of the Society for Neuroscience 31, 15703-15715.

Miquel, E., Cassina, A., Martinez-Palma, L., Souza, J.M., Bolatto, C., Rodriguez-Bottero, S., Logan, A., Smith, R.A., Murphy, M.P., Barbeito, L., et al. (2014). Neuroprotective effects of the mitochondria-targeted antioxidant MitoQ in a model of inherited amyotrophic lateral sclerosis. Free Radic Biol Med 70, 204-213.

Moffett, J.R., Arun, P., Ariyannur, P.S., and Namboodiri, A.M. (2013). N-Acetylaspartate reductions in brain injury: impact on post-injury neuroenergetics, lipid synthesis, and protein acetylation. Front Neuroenergetics 5, 11.

Orr, H.T. (2012). Cell biology of spinocerebellar ataxia. J Cell Biol 197, 167-177.

Overk, C.R., and Masliah, E. (2014). Pathogenesis of synaptic degeneration in Alzheimer's disease and Lewy body disease. Biochem Pharmacol 88, 508-516.

Oz, G., Nelson, C.D., Koski, D.M., Henry, P.G., Marjanska, M., Deelchand, D.K., Shanley, R., Eberly, L.E., Orr, H.T., and Clark, H.B. (2010). Noninvasive detection of presymptomatic and progressive neurodegeneration in a mouse model of spinocerebellar ataxia type 1. The Journal of neuroscience : the official journal of the Society for Neuroscience 30, 3831-3838.

Pellistri, F., Bucciantini, M., Invernizzi, G., Gatta, E., Penco, A., Frana, A.M., Nosi, D., Relini, A., Regonesi, M.E., Gliozzi, A., et al. (2013). Different ataxin-3 amyloid aggregates induce intracellular Ca(2+) deregulation by different mechanisms in cerebellar granule cells. Biochimica et biophysica acta 1833, 3155-3165.

Peng, T.I., and Jou, M.J. (2010). Oxidative stress caused by mitochondrial calcium overload. Ann N Y Acad Sci 1201, 183-188.

Pettersen, E.F., Goddard, T.D., Huang, C.C., Couch, G.S., Greenblatt, D.M., Meng, E.C., and Ferrin, T.E. (2004). UCSF Chimera--a visualization system for exploratory research and analysis. J Comput Chem 25, 1605-1612.

Rodriguez-Cuenca, S., Cocheme, H.M., Logan, A., Abakumova, I., Prime, T.A., Rose, C., Vidal-Puig, A., Smith, A.C., Rubinsztein, D.C., Fearnley, I.M., et al. (2010). Consequences of long-term oral administration of the mitochondria-targeted antioxidant MitoQ to wild-type mice. Free Radic Biol Med 48, 161-172.

Ross, J.M. (2011). Visualization of mitochondrial respiratory function using cytochrome c oxidase/succinate dehydrogenase (COX/SDH) double-labeling histochemistry. J Vis Exp, e3266.

Ruegsegger, C., Stucki, D.M., Steiner, S., Angliker, N., Radecke, J., Keller, E., Zuber, B., Ruegg, M.A., and Saxena, S. (2016). Impaired mTORC1-Dependent Expression of Homer-3 Influences SCA1 Pathophysiology. Neuron 89, 129-146.

Ruffoli, R., Bartalucci, A., Frati, A., and Fornai, F. (2015). Ultrastructural studies of ALS mitochondria connect altered function and permeability with defects of mitophagy and mitochondriogenesis. Front Cell Neurosci 9, 341.

Ryan, B.J., Hoek, S., Fon, E.A., and Wade-Martins, R. (2015). Mitochondrial dysfunction and mitophagy in Parkinson's: from familial to sporadic disease. Trends Biochem Sci 40, 200-210.

Schapira, A.H. (1996). Oxidative stress and mitochondrial dysfunction in neurodegeneration. Curr Opin Neurol 9, 260-264.

Schapira, A.H. (1998). Mitochondrial dysfunction in neurodegenerative disorders. Biochimica et biophysica acta 1366, 225-233.

Serra, H.G., Byam, C.E., Lande, J.D., Tousey, S.K., Zoghbi, H.Y., and Orr, H.T. (2004). Gene profiling links SCA1 pathophysiology to glutamate signaling in Purkinje cells of transgenic mice. Human molecular genetics 13, 2535-2543.

Signoretti, S., Marmarou, A., Aygok, G.A., Fatouros, P.P., Portella, G., and Bullock, R.M. (2008). Assessment of mitochondrial impairment in traumatic brain injury using high-resolution proton magnetic resonance spectroscopy. J Neurosurg 108, 42-52.

Simon, D.K., Zheng, K., Velazquez, L., Santos, N., Almaguer, L., Figueroa, K.P., and Pulst, S.M. (2007). Mitochondrial complex I gene variant associated with early age at onset in spinocerebellar ataxia type 2. Arch Neurol 64, 1042-1044.

Simoncini, C., Orsucci, D., Caldarazzo Ienco, E., Siciliano, G., Bonuccelli, U., and Mancuso, M. (2015). Alzheimer's pathogenesis and its link to the mitochondrion. Oxid Med Cell Longev 2015, 803942.

Smith, R.A., and Murphy, M.P. (2010). Animal and human studies with the mitochondria-targeted antioxidant MitoQ. Ann N Y Acad Sci 1201, 96-103.

Snow, B.J., Rolfe, F.L., Lockhart, M.M., Frampton, C.M., O'Sullivan, J.D., Fung, V., Smith, R.A., Murphy, M.P., Taylor, K.M., and Protect Study, G. (2010). A double-blind, placebo-controlled study to assess the mitochondria-targeted antioxidant MitoQ as a disease-modifying therapy in Parkinson's disease. Mov Disord 25, 1670-1674.

Tatsuta, T., and Langer, T. (2008). Quality control of mitochondria: protection against neurodegeneration and ageing. The EMBO journal 27, 306-314.

Travacio, M., Maria Polo, J., and Llesuy, S. (2000). Chromium(VI) induces oxidative stress in the mouse brain. Toxicology 150, 137-146.

Tsunemi, T., and La Spada, A.R. (2012). PGC-1alpha at the intersection of bioenergetics regulation and neuron function: from Huntington's disease to Parkinson's disease and beyond. Prog Neurobiol 97, 142-151.

Wang, L., Yang, X., and Shen, Y. (2015). Molecular mechanism of mitochondrial calcium uptake. Cellular and molecular life sciences : CMLS 72, 1489-1498.

Wang, Y.C., Lee, C.M., Lee, L.C., Tung, L.C., Hsieh-Li, H.M., Lee-Chen, G.J., and Su, M.T. (2011). Mitochondrial dysfunction and oxidative stress contribute to the pathogenesis of spinocerebellar ataxia type 12 (SCA12). The Journal of biological chemistry 286, 21742-21754.

Watase, K., Weeber, E.J., Xu, B., Antalffy, B., Yuva-Paylor, L., Hashimoto, K., Kano, M., Atkinson, R., Sun, Y., Armstrong, D.L., et al. (2002). A long CAG repeat in the mouse Sca1 locus replicates SCA1 features and reveals the impact of protein solubility on selective neurodegeneration. Neuron 34, 905-919.

Yu, Y.C., Kuo, C.L., Cheng, W.L., Liu, C.S., and Hsieh, M. (2009). Decreased antioxidant enzyme activity and increased mitochondrial DNA damage in cellular models of Machado-Joseph disease. J Neurosci Res 87, 1884-1891.

Zeviani, M., Simonati, A., and Bindoff, L.A. (2012). Ataxia in mitochondrial disorders. Handb Clin Neurol 103, 359-372.

Zoghbi, H.Y. (1995). Analysis of the CAG repeat and gene product in spinocerebellar ataxia type 1. Proceedings of the Association of American Physicians 107, 231-236.

Zoghbi, H.Y., and Orr, H.T. (1995). Spinocerebellar ataxia type 1. Seminars in cell biology 6, 29-35.

Zoghbi, H.Y., and Orr, H.T. (2009). Pathogenic mechanisms of a polyglutamine-mediated neurodegenerative disease, spinocerebellar ataxia type 1. The Journal of biological chemistry 284, 7425-7429.

Figure 1. Mass spectrometry analysis identifies mitochondrial impairments in mutant Sca1$^{154Q/2Q}$ PCs

(A) Using LCM, PCs were isolated and analyzed by MS. Of the 340 proteins reliably detected from two separate experiments, nearly 41% of the proteins displayed consistent ≥ 2 fold alteration alterations in expression levels in P100, Sca1$^{154Q/2Q}$ vs. WT PCs. Only proteins with a minimum PMSS of 30 and 3 or more unique peptides and detected in two separate experiments were analyzed. n = 4 mice per genotype per experiment.

(B) PANTHER overrepresentation analysis for pathways changed at P100 in Sca1$^{154Q/2Q}$ vs. WT PCs presenting enrichment for ATP synthesis and synaptic vesicle trafficking proteins. Protein classes which were significantly altered involved anion channels and members of the oxidoreductase family of proteins.

(C) 33% of the changed proteins in Sca1$^{154Q/2Q}$ PC proteome were downregulated at P100 and grouped according to protein classes after PANTHER analysis.

(D and **E)** Analysis of the PC proteome at P100. Strongest alterations in Sca1$^{154Q/2Q}$ PC proteome were for ATP synthesis (D) and for proteins functioning as oxidoreductase, involving the use utilization of NADP or NAD^+ as cofactors for catalyzing the transfer of electrons from one molecule, electron donor (reductant), to electron acceptor (oxidant) (E). Data plotted by PMSS score (only proteins reproducibly altered in 2 experiments were analyzed, PMSS values plotted for one experiment).

Figure 2. PCs of symptomatic Sca1$^{154Q/2Q}$ mice show altered mitochondrial morphology

(A) Immunolabeling for HSP60 (Mitochondrial marker) and Calbindin (PC maker) revealing an increased number of vesicular (spherical) shaped mitochondria in PCs of Sca1$^{154Q/2Q}$ mice at symptomatic stages P110 and P150, but not earlier.

(B) Left: Histogram for the mitochondrial distribution according to their sphericity value at P110. Right: Quantitative analysis (Q.A.) representing the proportion of mitochondria falling below or above a critical sphericity value (median of WT mice). n = 4 mice per genotype at P60 and P150, 5 mice per genotype at P110 (8-12 cells per individual mouse).

(C) SBF-SEM images rendered for mitochondria demonstrating that mitochondria of Sca1$^{154Q/2Q}$ PCs were shorter in length.

(D) Left: Histogram for the mitochondrial distribution according to their lengths. Right: Q.A. representing the proportion of mitochondria falling below or above a critical length (median of WT mice). n = 8 cells (250 mitochondria each) per genotype (3 mice each). Unpaired t test *p<0.05, **p<0.01, ***p<0.001. Scale bar: 10µm.

Figure 3. Reduced ETC complex I, II, IV and V activities in PCs of symptomatic Sca1$^{154Q/2Q}$ mice

Colorimetric assay in fresh thin cerebellar sections revealing decreased ETC complex I **(A)**, II **(B)**, IV **(C)** and V **(D)** staining intensities in PC somas of P110, Sca1$^{154Q/2Q}$ mice. ML: Molecular layer, PL: Purkinje cell layer, GL: Granule cell layer. Q.A. is presented as box with whiskers (Turkey). n = 43-80 sections (average) per genotype and assay (3 mice per genotype for Complex I and V, 4 mice per genotype for Complex II and IV). Unpaired t test *p<0.05, **p<0.01, ***p<0.001. Scale bar: 50µm.

Figure 4. Oxidative stress correlates with mitochondrial impairments in Sca1$^{154Q/2Q}$ mice

(A) Induction of oxidative stress by 3d chromium(VI) treatment led to an increased number of vesicular shaped mitochondria in WT PCs.

(B) ETC complex I and IV staining intensities were reduced after a 3d chromium(VI) treatment.). n = 30-50 sections (average) per genotype and assay (2 mice per genotype)

(C) Immunolabeling for 8-OHdG and Calbindin indicating increased oxidative stress in Sca1$^{154Q/2Q}$ PCs at symptomatic stages P110, but not earlier (P60).

(D) Q.A. is presented as box with whiskers (Turkey). n = 9-12 sections (average) per age and genotype (4 mice each). Unpaired t test *p<0.05, **p<0.01, ***p<0.001. Scale bars: (A) = 10µm, (B) = 50µm and (C) = 20µm.

Figure 5. MitoQ treatment ameliorates mitochondrial morphological impairments in PCs of Sca1$^{154Q/2Q}$ mice

(A) Immunolabeling for HSP60 and Calbindin at P150 demonstrating numerous vesicular shaped mitochondria (arrowheads) in Sca1$^{154Q/2Q}$ control PCs. “Long term” MitoQ treatment from P40-150 restored mitochondrial morphology in PCs of P150, Sca1$^{154Q/2Q}$ mice and did not have an effect on P150, WT animals.

(B) Q.A. representing the proportion of mitochondria falling below or above a critical sphericity value (median of WT control mice). n = 4 mice [WT control], 3 mice [150, WT MitoQ trt P40-150], 4 mice [Sca1$^{154Q/2Q}$ control], 4 mice [Sca1$^{154Q/2Q}$ MitoQ trt P40-150] (6-12 cells per individual mouse).

(C) HSP60 and Calbindin immunolabeling at P110 presenting numerous vesicular shaped mitochondria (arrowheads) in PCs of SCA1$^{154Q/2Q}$ control mice. “Short term” MitoQ treatment from P90-P110 restored mitochondrial morphology in P110, Sca1$^{154Q/2Q}$ PCs.

(D) Q.A. presenting the proportion of mitochondria falling below or above a critical sphericity value (median of WT mice). n = 5 mice [WT control], 5 mice [Sca1$^{154Q/2Q}$ control] and 3 mice [Sca1$^{154Q/2Q}$ MitoQ trt P90-110] (6-12 cells per individual mouse).

(E) SBF-SEM images rendered for mitochondria demonstrating that mitochondria of Sca1$^{154Q/2Q}$ MitoQ trt P90-110 and WT PCs had similar lengths.

(F) Left: Histogram for the mitochondrial distribution according to their lengths. Right: Q.A. representing the proportion of mitochondria falling below or above a critical length (median of WT mice). n = 8 cells (250 mitochondria each) per genotype (3 mice each). One-way ANOVA

with post hoc Bonferroni's test (B and D), unpaired t test (F) *p<0.05, **p<0.01, ***p<0.001. Scale bar: 10µm.

Figure 6. Long term MitoQ treatment of Sca1$^{154Q/2Q}$ mice from P40-150 restores functionality of ETC complexes I, II, IV and V

Colorimetric assay for complex I **(A)**, II **(B)**, IV **(C)** and V **(D)** activities in fresh thin cerebellar sections displayed significant reduced staining intensities in PCs of P150, SCA1$^{154Q/2Q}$ mice which were restored after MitoQ administration from P40-150. Q.A. is presented as box with whiskers (Turkey). n = 40-78 sections (average) per group (4 mice [WT control], 3 mice [WT MitoQ trt P40-150], 4 mice [Sca1$^{154Q/2Q}$ control] and 4 mice [Sca1$^{154Q/2Q}$ MitoQ trt P40-150]). One-way ANOVA with post hoc Bonferroni's test *p<0.05, **p<0.01, ***p<0.001. Scale bar: 20µm.

Figure 7. MitoQ treatment ameliorates motor coordination and PC neuropathology of symptomatic Sca1$^{154Q/2Q}$ mice

(A) Rotarod performance was measured for WT and Sca1$^{154Q/2Q}$ mice that were either untreated (control) or treated with MitoQ from P40-150 (MitoQ trt P40-150). Compared to WT control mice, Sca1$^{154Q/2Q}$ control animals exhibited significant differences in motor coordination from P110 on, whereas Sca1$^{154Q/2Q}$ MitoQ trt P40-150 mice did not display significant alterations until P150. MitoQ treatment did not have a significant effect on WT animals. n = 9 mice [WT control], 6 mice [WT MitoQ trt P40-150], 14 mice [Sca1$^{154Q/2Q}$ control] and 9 mice [Sca1$^{154Q/2Q}$ MitoQ trt P40-150].

(B) Hind-limb clasping performance is blotted via clasping score criteria (The higher score corresponds to worse phenotype). Compared to Sca1$^{154Q/2Q}$ control, Sca1$^{154Q/2Q}$ MitoQ trt P40-150 mice demonstrated an improved score at P110 (left) and P150 (right). MitoQ treatment did not have an effect on WT mice. n = 6 mice [WT control], 6 mice [WT MitoQ trt P40-150], 6 mice [Sca1$^{154Q/2Q}$ control] and 9 mice [Sca1$^{154Q/2Q}$ MitoQ trt P40-150].

(C) Quantified Calbindin intensities, averaged and blotted from the perikaryon center over the dendrites, presenting decreased levels in Sca1$^{154Q/2Q}$ control compared to WT control mice, which were restored after MitoQ treatment from P40-150 (left) and P90-110 (right).

(D) PC number over 315 µm was quantified in lobule V revealing reduced PCs in Sca1$^{154Q/2Q}$ control mice. Both, MitoQ administration from P40-150 (left) and P90-110 (right) prevented PC loss in Sca1$^{154Q/2Q}$ animals. n = 12-30 section per group (P150: 5 mice [WT control], 3 mice [WT MitoQ trt P40-150], 5 mice [Sca1$^{154Q/2Q}$ control] and 4 mice [Sca1$^{154Q/2Q}$ MitoQ trt P40-150]; P110: 7 mice [WT control], 5 mice [Sca1$^{154Q/2Q}$ control] and 3 mice [Sca1$^{154Q/2Q}$ MitoQ trt P90-

110] (C and D). Two-way ANOVA with post hoc Bonferroni's test (A), One-way ANOVA with post hoc Bonferroni's test for (B and D) *p<0.05, **p<0.01, ***p<0.001.

Suppl. Figure 1. Schematic representation of PC mitochondrial isosurface.

A representative image showing immunohistomchemical labeling of mitochondria in P110, WT and Sca1$^{154Q/2Q}$ PCs and its corresponding isosurface buildup using Imaris 7.6. Scale bar: 10µm.

Suppl. Figure 2. Short term MitoQ treatment from P90-110 improves ETC complex activities Sca1$^{154Q/2Q}$ PCs and reduces levels of oxidative stress marker 8OHdG

Colorimetric assay for ETC complex I **(A)**, II **(B)**, IV **(C)** and IV **(D)** activities displays reduced intensity levels in PCs of Sca1$^{154Q/2Q}$ control mice and that MitoQ administration from P90-100 reverses this effect. Q.A. is presented as box with whiskers (Turkey). n = 34-80 sections (average) per group (4 mice [WT control], 4 mice [Sca1$^{154Q/2Q}$ control] and 3 mice [Sca1$^{154Q/2Q}$ MitoQ trt P90-110] for Complex II and IV; 3 mice [WT control], 3 mice [Sca1$^{154Q/2Q}$ control] and 3 mice [Sca1$^{154Q/2Q}$ MitoQ trt P90-110] for Complex I and V.

(E) P110, Sca1$^{154Q/2Q}$ control mice display elevated 8-OHdG levels which is restored after the treatment with MitoQ from P90-110. Q.A. is presented as box with whiskers (Turkey). n = 9-12 sections (average) per group (4 mice [WT control], 4 mice [Sca1$^{154Q/2Q}$ control] and 3 mice [Sca1$^{154Q/2Q}$ MitoQ trt P90-110]). One-way ANOVA with post hoc Bonferroni's test *p<0.05, **p<0.01, ***p<0.001. Scale bars: (A-D) = 50 µm and (E) = 20µm.

Table S1 related to main Figure 1.

Complete list of proteins identified by MS which were altered in mutant PCs from Sca1$^{154Q/2Q}$ mice compared to WT mice.

Highlights

- Morphological and functional mitochondrial alterations in SCA1 Purkinje cells
- Mitochondrial impairments coincides with elevated levels of oxidative stress
- Administration of antioxidant MitoQ to SCA1 mice ameliorates mitochondrial deficits
- Restoring mitochondrial function improves motor coordination and neuropathology

Fig. 1

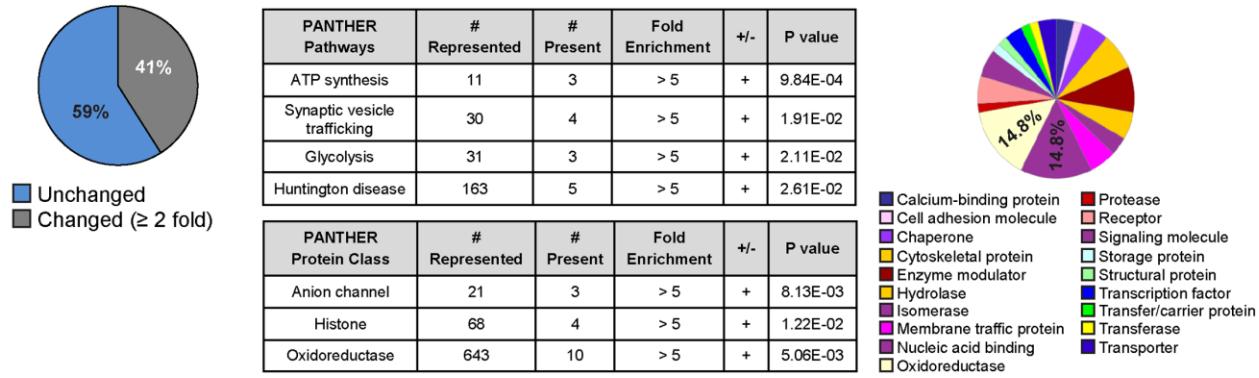

PANTHER Pathways	# Represented	# Present	Fold Enrichment	+/-	P value
ATP synthesis	11	3	> 5	+	9.84E-04
Synaptic vesicle trafficking	30	4	> 5	+	1.91E-02
Glycolysis	31	3	> 5	+	2.11E-02
Huntington disease	163	5	> 5	+	2.61E-02

PANTHER Protein Class	# Represented	# Present	Fold Enrichment	+/-	P value
Anion channel	21	3	> 5	+	8.13E-03
Histone	68	4	> 5	+	1.22E-02
Oxidoreductase	643	10	> 5	+	5.06E-03

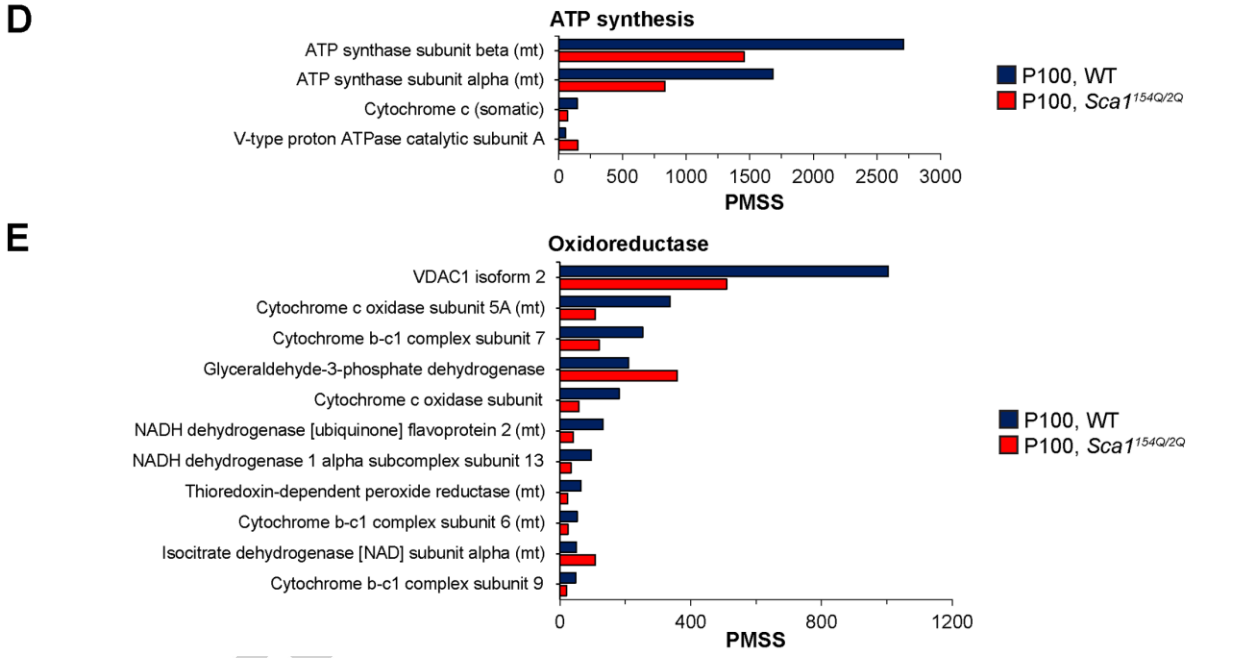

Fig. 2

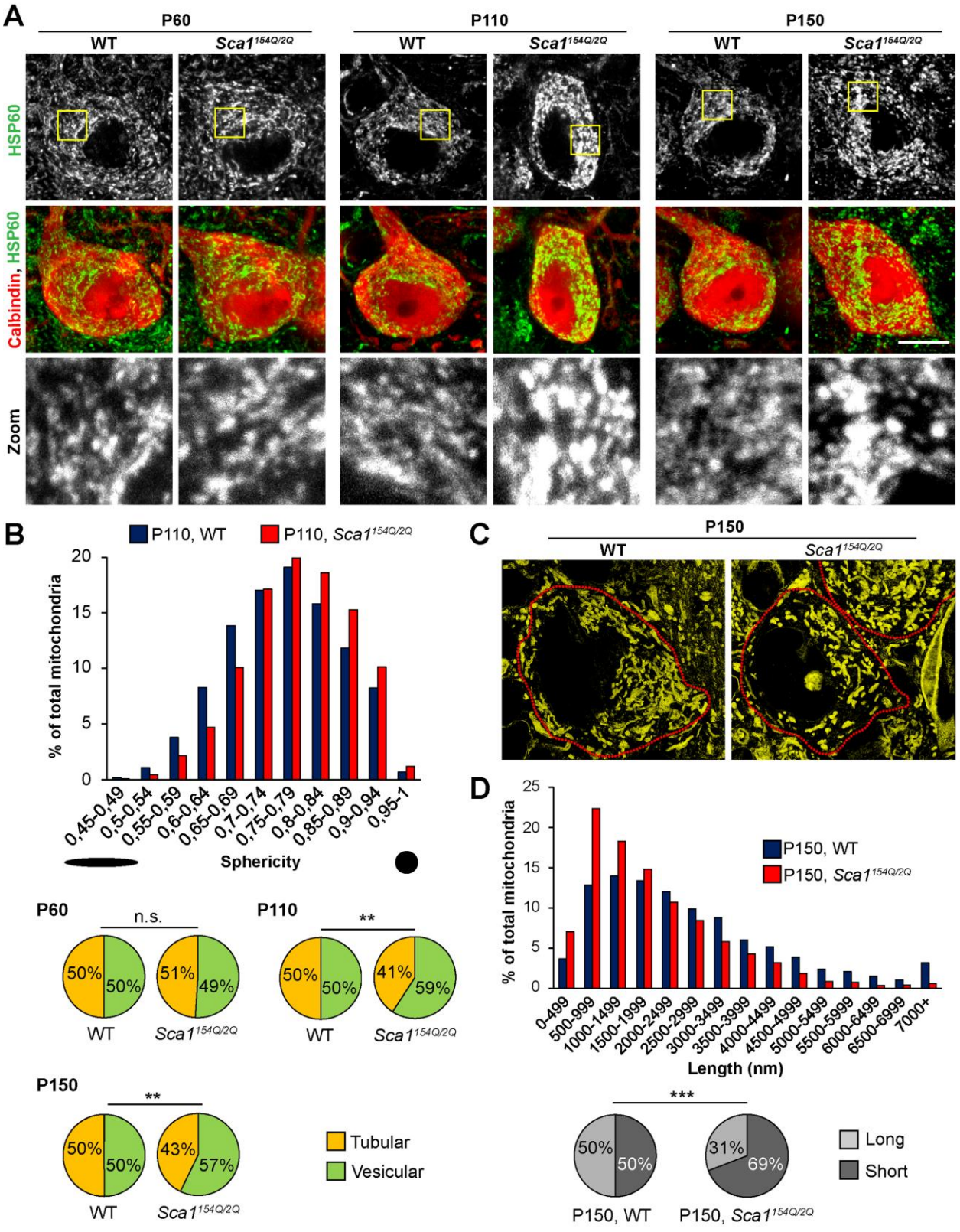
A
P60
P110
P150
WT
Sca1154Q/2Q
HSP60
Calbindin, HSP60
Zoom
B
P110, WT
P110, Sca1154Q/2Q
% of total mitochondria
Sphericity
0,45-0,49
0,5-0,54
0,55-0,59
0,6-0,64
0,65-0,69
0,7-0,74
0,75-0,79
0,8-0,84
0,85-0,89
0,9-0,94
0,95-1
P60
n.s.
50%
50%
51%
49%
P110
**
50%
50%
41%
59%
P150
**
50%
50%
43%
57%
Tubular
Vesicular
C
P150
WT
Sca1154Q/2Q
D
P150, WT
P150, Sca1154Q/2Q
% of total mitochondria
Length (nm)
0-499
500-999
1000-1499
1500-1999
2000-2499
2500-2999
3000-3499
3500-3999
4000-4499
4500-4999
5000-5499
5500-5999
6000-6499
6500-6999
7000+
***
50%
50%
31%
69%
Long
Short
P150, WT
P150, Sca1154Q/2Q

Fig. 3

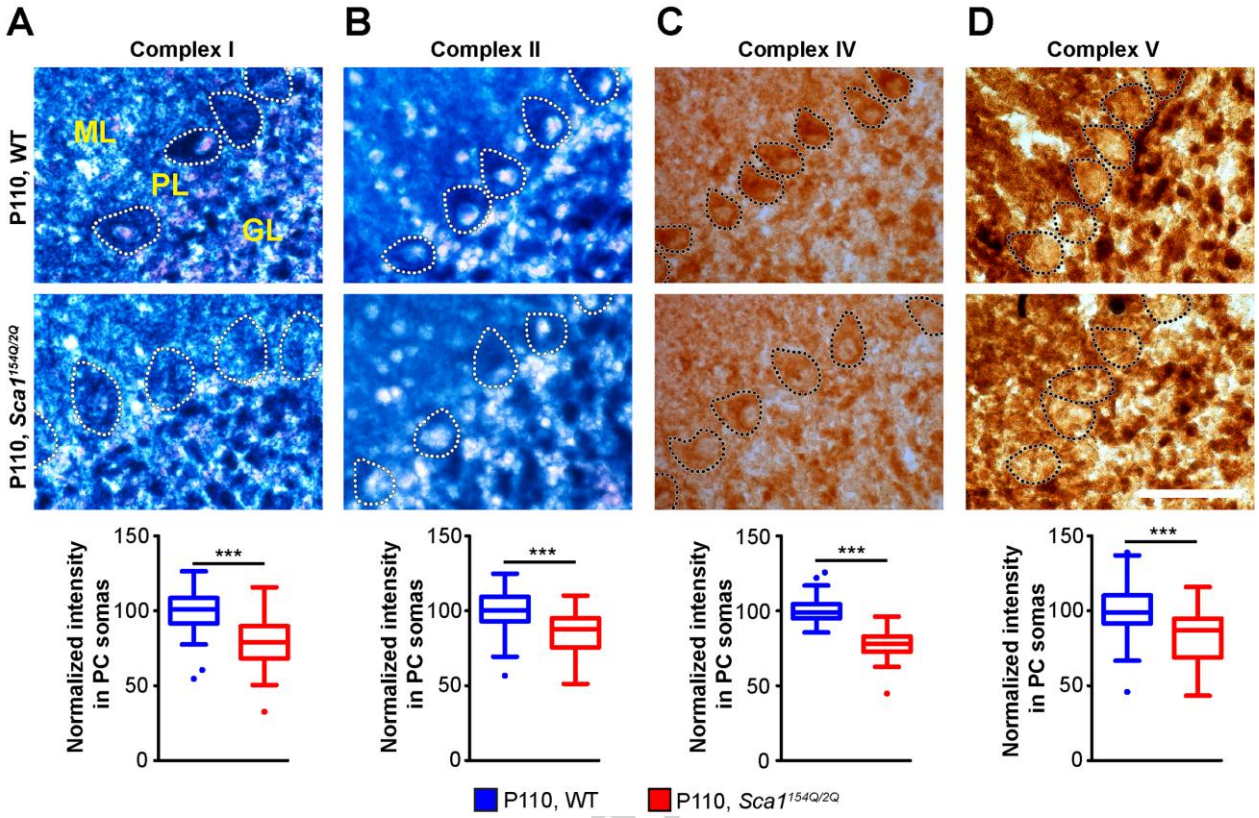

Fig. 4

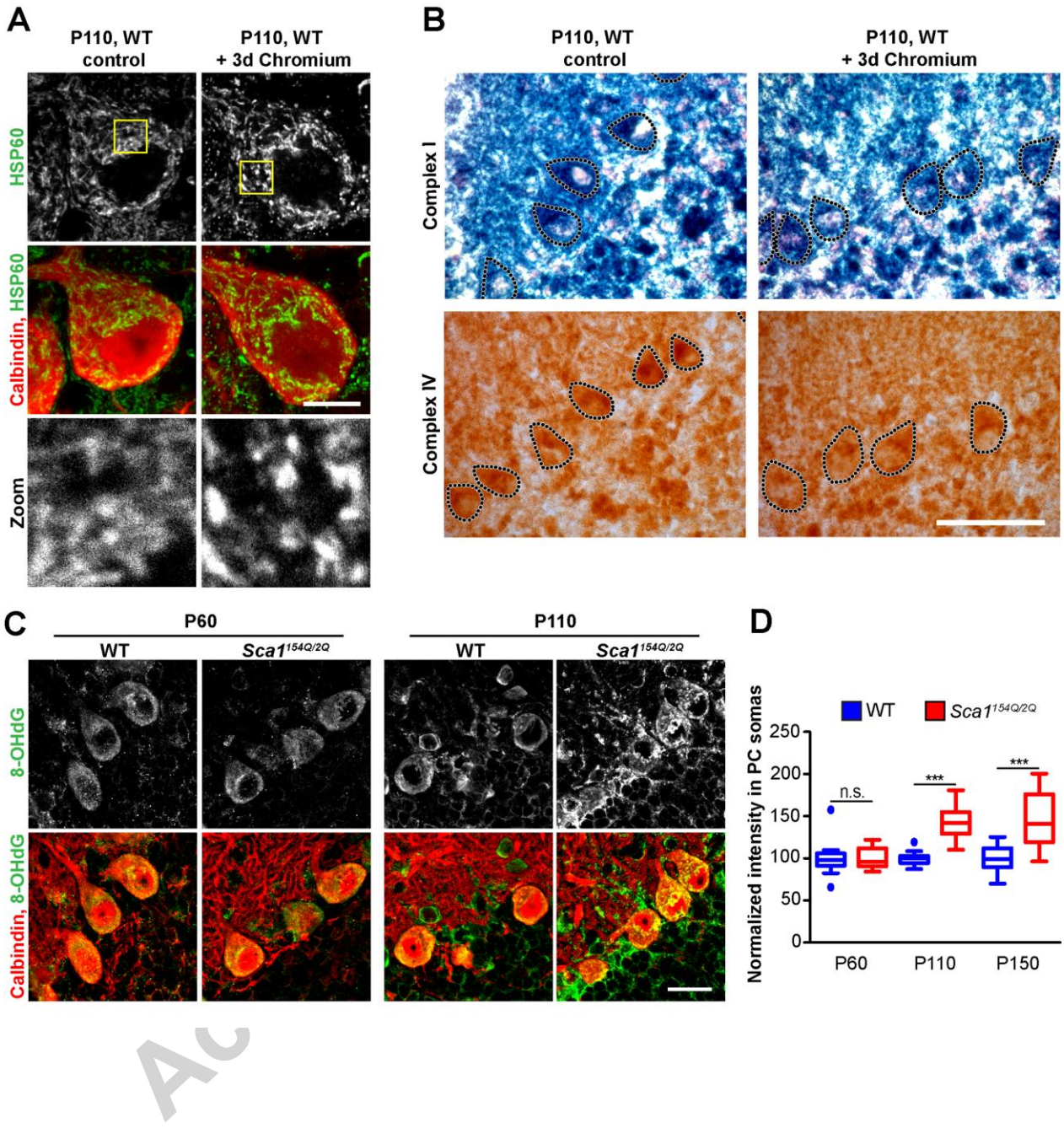
A
P110, WT control
P110, WT + 3d Chromium
HSP60
Calbindin, HSP60
Zoom
B
P110, WT control
P110, WT + 3d Chromium
Complex I
Complex IV
C
P60
P110
WT
Sca1154Q/2Q
8-OHdG
Calbindin, 8-OHdG
D
WT
Sca1154Q/2Q
Normalized intensity in PC somas
250
200
150
100
50
0
n.s.
***
***
P60
P110
P150

Fig. 5

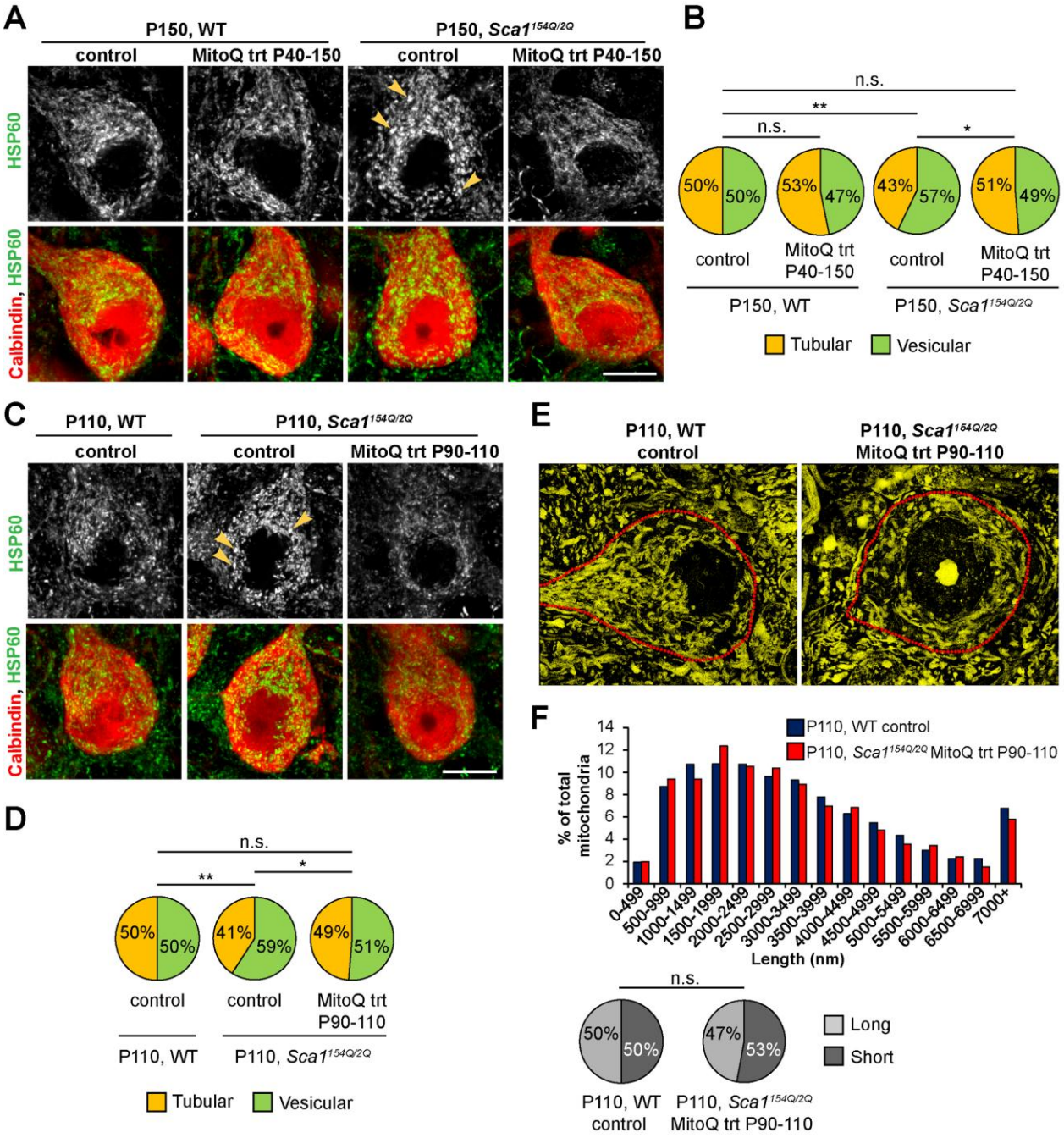
A
P150, WT
P150, Sca1154Q/2Q
control
MitoQ trt P40-150
control
MitoQ trt P40-150
HSP60
Calbindin, HSP60
B
n.s.
**
n.s.
*
50%
50%
53%
47%
43%
57%
51%
49%
control
MitoQ trt P40-150
control
MitoQ trt P40-150
P150, WT
P150, Sca1154Q/2Q
Tubular
Vesicular
C
P110, WT
P110, Sca1154Q/2Q
control
control
MitoQ trt P90-110
HSP60
Calbindin, HSP60
D
n.s.
**
*
50%
50%
41%
59%
49%
51%
control
control
MitoQ trt P90-110
P110, WT
P110, Sca1154Q/2Q
Tubular
Vesicular
E
P110, WT control
P110, Sca1154Q/2Q MitoQ trt P90-110
F
P110, WT control
P110, Sca1154Q/2Q MitoQ trt P90-110
% of total mitochondria
0
2
4
6
8
10
12
14
0-499
500-999
1000-1499
1500-1999
2000-2499
2500-2999
3000-3499
3500-3999
4000-4499
4500-4999
5000-5499
5500-5999
6000-6499
6500-6999
7000+
Length (nm)
n.s.
50%
50%
47%
53%
Long
Short
P110, WT control
P110, Sca1154Q/2Q MitoQ trt P90-110

Fig. 6

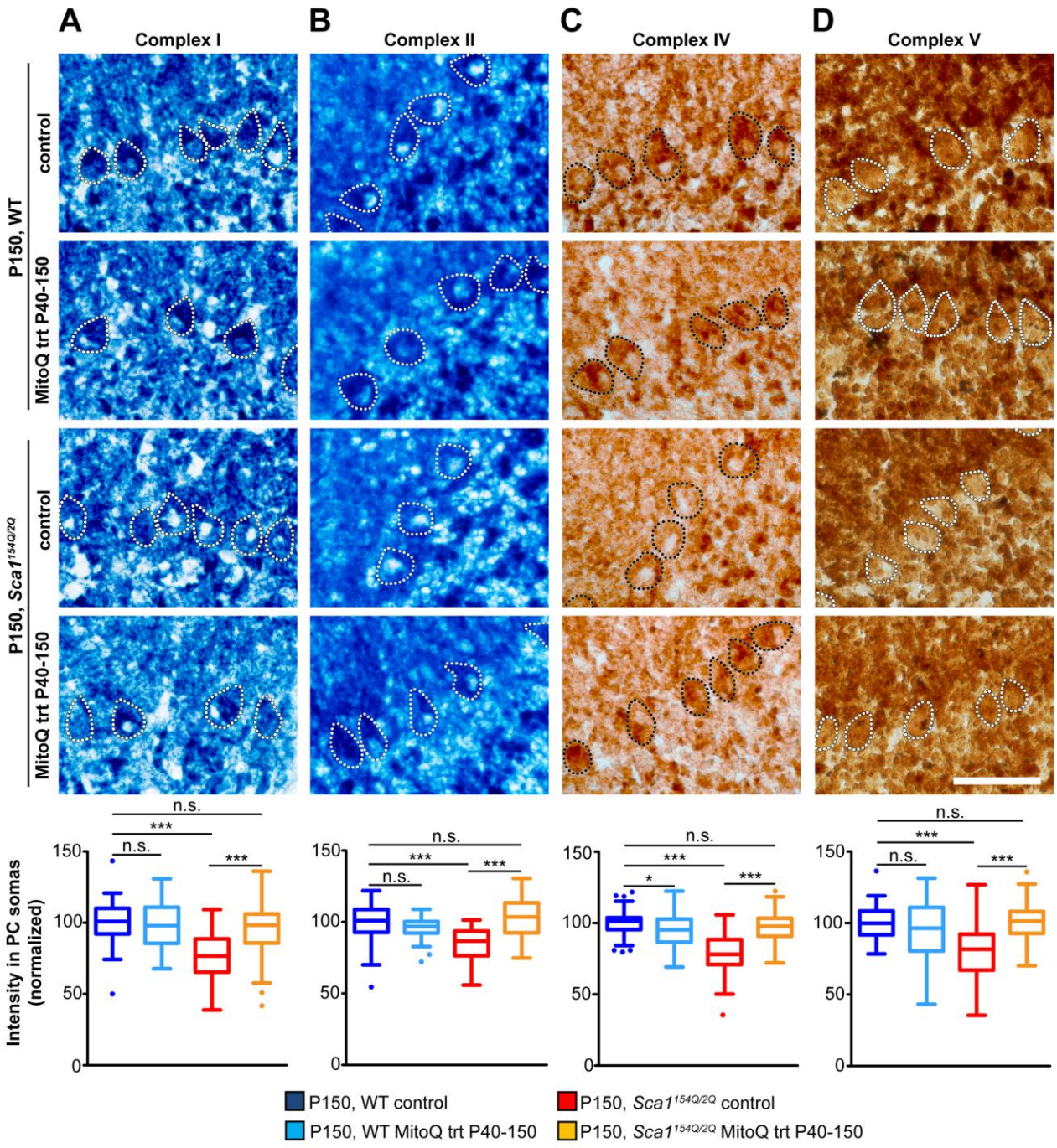
A
Complex I
B
Complex II
C
Complex IV
D
Complex V
P150, WT
control
MitoQ trt P40-150
P150, Sca1154Q/2Q
control
MitoQ trt P40-150
Intensity in PC somas (normalized)
150
100
50
0
n.s.
***
n.s.
***
*
P150, WT control
P150, WT MitoQ trt P40-150
P150, Sca1154Q/2Q control
P150, Sca1154Q/2Q MitoQ trt P40-150

Fig. 7

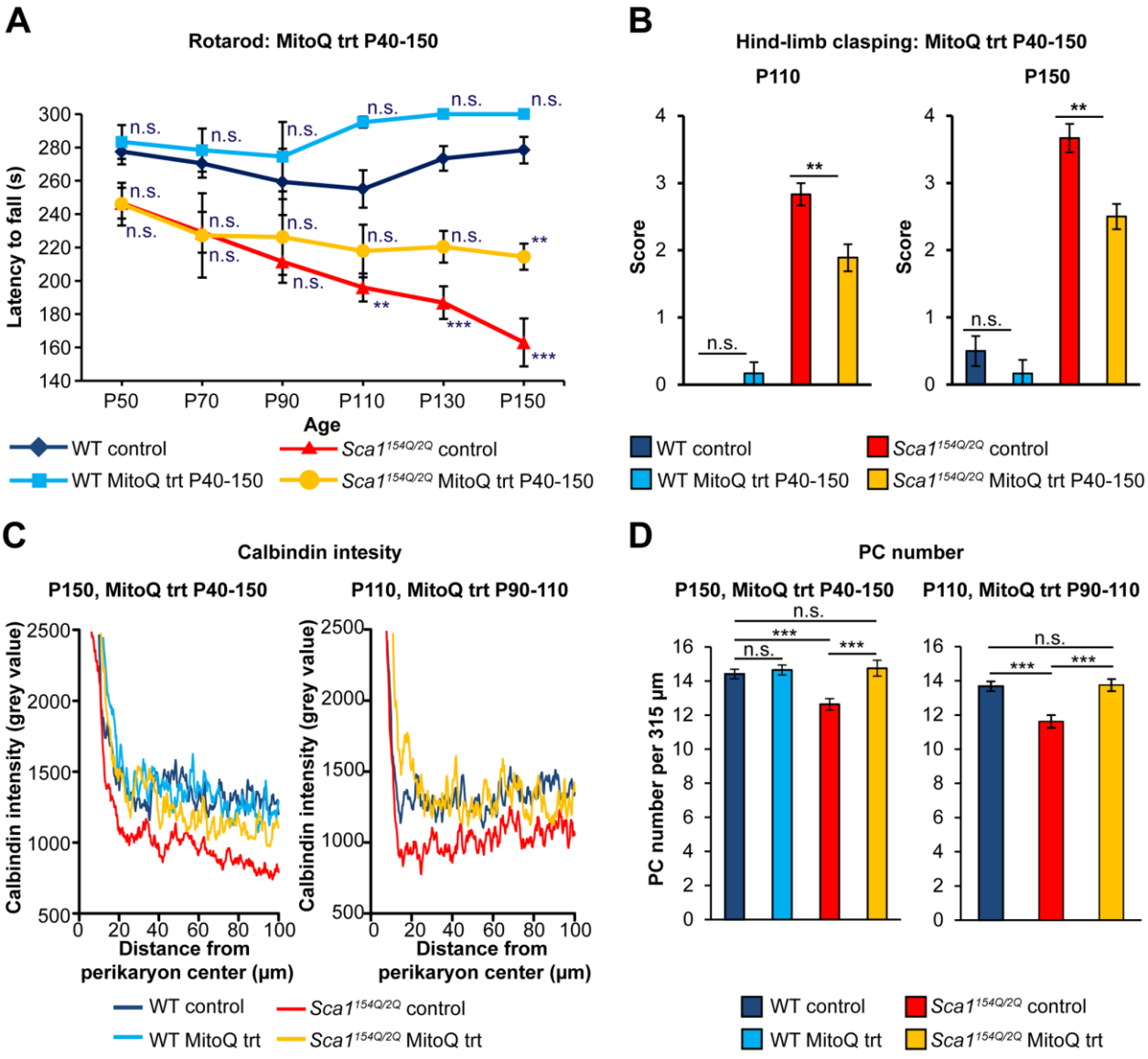
A
Rotarod: MitoQ trt P40-150
Latency to fall (s)
Age
P50
P70
P90
P110
P130
P150
WT control
WT MitoQ trt P40-150
Sca1154Q/2Q control
Sca1154Q/2Q MitoQ trt P40-150
B
Hind-limb clasping: MitoQ trt P40-150
P110
P150
Score
C
Calbindin intesity
P150, MitoQ trt P40-150
P110, MitoQ trt P90-110
Calbindin intensity (grey value)
Distance from perikaryon center (µm)
WT control
WT MitoQ trt
Sca1154Q/2Q control
Sca1154Q/2Q MitoQ trt
D
PC number
P150, MitoQ trt P40-150
P110, MitoQ trt P90-110
PC number per 315 µm
WT control
WT MitoQ trt
Sca1154Q/2Q control
Sca1154Q/2Q MitoQ trt